Assignments for the Main-Chain Nuclear Magnetic Resonances and Delineation of the Secondary Structure of the Catalytic Domain of Human Stromelysin-1 As Obtained from Triple-Resonance 3D NMR Experiments

Steven R. Van Doren,[‡] Alexander V. Kurochkin,[‡] Qi-Zhuang Ye,*[,§] Linda L. Johnson,[§] Donald J. Hupe,[§] and Erik R. P. Zuiderweg*[,‡]

Biophysics Research Division and Department of Biological Chemistry, The University of Michigan, 930 North University, Ann Arbor, Michigan 48109-1055, and Department of Biochemistry, Parke-Davis Pharmaceutical Research, Warner-Lambert Company, 2800 Plymouth Road, Ann Arbor, Michigan 48105

Received July 16, 1993; Revised Manuscript Received September 7, 1993[⊗]

ABSTRACT: We report the NMR assignments for the main-chain ^{13}C, ^{15}N, and ^{1}H resonances (^{1}HN, $^{1}H^{\alpha}$, $^{15}N^{\alpha}$, $^{13}C^{\alpha}$, ^{13}CO) for the 19.5-kDa catalytic domain of human stromelysin-1, a zinc endoproteinase thought to be involved in pathologic tissue degradation. The assignments were predominantly obtained from triple-resonance three-dimensional NMR experiments using double-labeled ($^{15}N/^{13}C$) samples. The secondary structure of the molecule was determined from analysis of 3D ^{15}N-resolved NOESY experiments. It was found to consist of a five-stranded mixed β-sheet with four parallel and one antiparallel strand and three helices. The topological arrangement of the secondary structure elements of stromelysin catalytic domain is remarkably similar to that found for astacin, a Zn proteinase for which the tertiary structure was recently determined from X-ray diffraction data [Bode et al. (1992) *Nature 358*, 164–167].

Human stromelysin-1 belongs to a family of matrix (zinc) metalloproteinases involved in the remodeling of the extracellular matrix as occurs during embryonic bone and growth plate development, ovulation, and wound healing. The enzyme is thought to participate in the proteolysis associated with rheumatoid arthritis and osteoarthritis and with cancer metastasis [for reviews see Emonard and Grimaud (1990), Woessner (1991), and Matrisian (1992)]. Stromelysin-1 is a wide-spectrum zinc endoproteinase of molecular mass 52 kDa, that hydrolyzes types III, IV, V, and IX collagen, gelatins, fibronectin, laminin, and several cartilage proteoglycans. Stromelysin can participate in activation of itself and of other matrix metalloproteinases such as collagenases and gelatinases (Nagase et al., 1991; Miyazaki et al., 1992) by lysis of X–Phe bonds, thereby removing the prosequences of these enzymes. It specifically cleaves human aggrecan at a Asn–Phe bond (Flannery et al., 1992) and macroglobulins at Gly–Leu and Phe–Tyr bonds (Enghild et al., 1989). Substrate specificity is thus found to require a large hydrophobic residue at the C-terminal side of the scissile bond. Currently, three stromelysin molecules (stromelysin-1, -2 and -3; Matrisian, 1992) have been described. Stomelysins-1 and -2 are especially homologous.

Here we report on structural NMR studies of the catalytic domain of stromelysin-1. Stromelysin is expressed as a zymogen, is activated by itself and serine proteinases, and is inhibited in vivo by tissue inhibitors of metalloproteinases (TIMPs)[1] (Woessner, 1991; Matrisian, 1992; Murphy & Docherty, 1992). It appears that elevated levels of MMPs in general and stromelysins in particular are correlated with tumor metastasis and invasion caused by pathological degradation of the extracellular matrix: strongly elevated levels of matrix metalloroteinases (MMPs) including stromelysins have been found in a large fraction of breast carcinomas (Basset et al., 1990; Clavel et al., 1992) and in several tumorigenic cell lines (Stetler-Stevenson, 1990; Polette et al., 1991; Kusukawa, 1992). Metastatic behavior of oncogene-transformed rat cell lines has been strongly correlated with high levels of the stromelysins-1 and -2 (Sreenath, 1992; Engel et al., 1992). Enhanced activity of stromelysin-1 (MMP-3) was also observed in synovial tissues afflicted by rheumatoid arthritis or traumatic knee injury (Walakovits et al., 1992) and in cartilage and synovium afflicted by osteoarthritis (Okada et al., 1992). The family of MMP proteins as a whole is therefore an important target for antimetastasis and RA/OA drug research.

Three-dimensional structures of MMPs have not yet been published, nor for any other protein that shares significant overall amino acid homology (i.e., >10% identity) with these molecules. Crystal structures are known for thermolysin (Holmes et al., 1982) and astacin (Bode et al., 1992; Gomis-Rüth et al., 1993), both Zn endoproteinases. Amino acid homology between astacin and the MMPs has previously been detected only in the identity of 5 of 11 residues of the consensus zinc binding sequence (Stöcker et al., 1990; Bode et al., 1992). Three of these 11 putative active-site residues are also identical with those of thermolysin. In this stretch of 11, the third histidine, found in astacin and the MMPs, is not shared with thermolysin. This results in a profound difference between the structures of the active sites of thermolysin and astacin: Zn is 4-fold coordinated in thermolysin and 5-fold coordinated in astacin. Which coordination applies for the MMPs awaits reports of tertiary structure.

With a 52-kDa molecular mass, stromelysin is currently beyond the limits of NMR methodology for detailed studies. However, strong evidence supports the hypothesis that the N-terminal 20-kDa domain of the mature protein (Phe^{83}–Pro^{256}) is sufficient for full stromelysin catalytic activity.

* To whom correspondence should be addressed.
‡ The University of Michigan.
§ Warner-Lambert Co.
⊗ Abstract published in *Advance ACS Abstracts,* November 1, 1993.
[1] Abbreviations: SCD, human stromelysin-1 catalytic domain; rf, radio frequency; NOE, nuclear Overhauser effect; TIMP, tissue inhibitor of metalloproteinase; MMP, matrix metalloproteinase; RA, rheumatoid arthritis; OA, osteoarthritis.

0006-2960/93/0432-13109$04.00/0

Related 20-kDa domains are present in the other MMPs, as evidenced by a 44% amino acid identity between human matrilysin (the prototypical 20-kDa MMP) and collagenase and 49% between matrilysin and stromelysin in these areas. The domain structure was also suggested by the presence of shorter but active forms (22–30 kDa) of stromelysin (Nagase et al., 1990) and collagenase (Clark et al., 1989) in pure enzyme preparations, presumably caused by autolysis. We (Ye et al., 1992) and others (Marcy et al., 1991) have constructed a 19.5-kDa "catalytic domain" of human stromelysin-1 (SCD). The enzymatic activity of this construct was shown to be essentially identical to that of full-length native stromelysin in cleavage of substance-P (Marcy et al., 1991), of thiopeptolide, and of its physiological substrate proteoglycan (Ye et al., 1992). A pH maximum (pH 6.0) of activity identical to that reported for full-length stromelysin was also reported by Ye et al. (1992). Inhibitors of full-length stromelysin (DiPasquale, 1986) were also found to inhibit SCD with the same potencies (Ye et al., 1993). Thus, the domain Phe^{83}–Pro^{256} of stromelysin (corresponding to the N-terminus of the mature protein) has been shown to be sufficient not only for catalytic activity, but also for specificity and inhibition.

As structure determination by NMR relies on distance constraints derived from NOEs between hydrogen atoms, multidimensional heteronuclear NMR approaches are required to obtain assignments for these nuclei from the overcrowded spectra of larger proteins. SCD is of a size (174 amino acid residues, 19.5 kDa) amenable to modern multinuclear multidimensional NMR. Resonance assignments have been obtained recently with such methods for proteins of approximately equal number of residues such as flavodoxin (Clubb et al., 1991), dihydrofolate reductase (Stockman et al., 1992), and calmodulin (Ikura et al., 1992). Main-chain assignments have also been reported for interferon γ, which is a dimer of molecular mass 32 kDa (Grzesiek et al., 1992). Full three-dimensional solution structures determined by modern heteronuclear NMR methods have been reported for calmodulin (Ikura et al., 1992), interleukin 1β (Clore et al., 1991), the complex of FK507 and FKBP (Meadows et al., 1993), and the complex of cyclosporin and cyclophilin (Theriault et al., 1993). This report represents the first stages of a similar analysis of stromelysin catalytic domain in which we describe the assignment of the resonances of the main-chain atoms and derive its secondary structure. The ultimate goal is to determine its three-dimensional structure in solution to help understand the architecture, catalytic mechanism, specificity, activation, and inhibition of stromelysin, as well as to help in the design of inhibitors. The catalytic domain of stromelysin was chosen for study because it is a *representative* member of the MMP family displaying the characteristics of specificity and activation, and because it is an *important* member of this family, implicated in tumor metastasis and in tissue damage in arthritis.

EXPERIMENTAL PROCEDURES

Expression and Purification of ^{15}N and $^{15}N/^{13}C$ Uniformly Labeled SCD. The construction of the SCD expression vector and the expression and purification of SCD have been described previously (Ye et al., 1992). The expression of SCD was controlled by a T7 promoter in the *Escherichia coli* strain DH5α. T7 RNA polymerase in this strain was provided by a second plasmid pGP1-2 (Tabor & Richardson, 1985). Fermentations were carried out in a 2-L fermenter equipped with pH monitor and automatic pH adjustment. Cultures were grown in either Celtone-N (^{15}N-labeling) or Celtone-CN (^{15}N, ^{13}C-labeling) (Martek Corp., Columbia, MD) supplemented with 0.01% thiamine, 50 μg/mL ampicillin, and 50 μg/mL kanamycin. The cells were cultured at 30 °C, and expression of SCD was induced at mid-log phase growth by increasing the temperature to 42 °C for 15 min. The temperature was lowered to 37 °C and SCD was allowed to express for 4–16 h, at pH 7.0–7.5 (pH was adjusted by phosphoric acid and ammonium hydroxide). Labeled SCD was purified from the insoluble fraction as previously described (Ye et al., 1992). The labeled proteins were analyzed by electrospray mass spectroscopy (Heath et al., 1993). Yields for the labeled protein were about 10–15 mg from the 2-L fermentation.

Preparation of Selectively Labeled SCD. Specific amino acids of SCD were labeled with ^{15}N using the method described by Hilber et al. (1989) with modifications. Each liter of M9 medium was supplemented with 0.1 g each of all L-amino acids except the amino acid to be labeled, 0.75% glucose, 1.0 g of adenine, 1.0 g of guanosine, 1.0 g of uracil, 0.4 g of thymine, 0.4 g of cytosine, 100 μg/mL kanamycin, 100 μg/mL ampicillin, and 1 mM IPTG. A 50-mL overnight culture in the supplemented M9 medium was used to inoculate a 2-L fermentation. This culture was grown at 30 °C to A600 of about 1.5. The ^{15}N-labeled L-amino acid phenylalanine or alanine (200 μg/mL) (obtained from Cambridge Isotope Laboratories) was added, and the expression of SCD was induced by raising the temperature to 42 °C. The cells were harvested after 2 h at 42 °C. Yields for selectively labeled SCD were from 2 to 6 mg from the 2-L fermentation. The *E. coli* strain we used was auxotrophic for leucine. To obtain SCD selectively labeled at leucine residues, the cells were grown in the same supplemented M9 medium with [^{15}N]-leucine added at the start of fermentation.

NMR Sample Preparation. To stabilize SCD for the long-term 3D and 4D NMR experiments required, a pH near neutrality and a Ca^{2+} concentration of at least 10 mM were found to be optimal. To alleviate aggregation of SCD, acetonitrile was added as a cosolvent. Samples at a concentration of 0.6–1.5 mM ^{15}N or $^{15}N/^{13}C$ (>95% uniform) SCD were dialyzed against 10 mM Tris-d_{11}·HCl (pH 7.0), 20 mM $CaCl_2$, 15% acetonitrile-d_3, and 8% D_2O. The deuterated compounds were obtained from Cambridge Isotope Laboratories. As a precaution against autolysis of SCD, a 2:1 excess of the hydroxamate inhibitor ICI-U24522, with an IC_{50} of about 40 nM (DiPasquale et al., 1986), was added to the samples. All spectra were collected at 32 °C.

NMR Spectroscopy. All triple-resonance experiments were carried out with U-(95–100%) $^{13}C/^{15}N$-labeled SCD on a Bruker AMX-600 NMR spectrometer operating at 14 T. The instrument is equipped with four rf channels, three of them standard, and one additional heteronuclear channel, consisting of synthesizer, gating network, and linear amplifier interfaced to the system as described previously (Van Doren & Zuiderweg, 1993). The experiments were carried out using a triple-resonance $^{15}N/^{13}C/^{1}H$ 5-mm probe with 1.0–1.5 mM samples of 0.5 mL except for the HA(CACO)NH, HA(CA)CO(N)H, and HNCO experiments, for which an 8-mm $^{15}N/^{13}C/^{1}H$ probe was used with a 0.6 mM sample of 1.2 mL. The gradient-enhanced ^{15}N-HSQC and ^{15}N-resolved NOESY-HSQC experiments were carried out with a 1.5 mM sample of 100% ^{15}N-labeled SCD using a Bruker AMX-500 spectrometer equipped with a Bruker GRASP unit and a gradient triple-resonance $^{15}N/^{13}C/^{1}H$ 5-mm probe.

The sequences used for the 2D ^{15}N gradient-enhanced, in-phase HSQC, 3D CT-HNCA, 3D CT-HN(CO)CA, 3D CT-

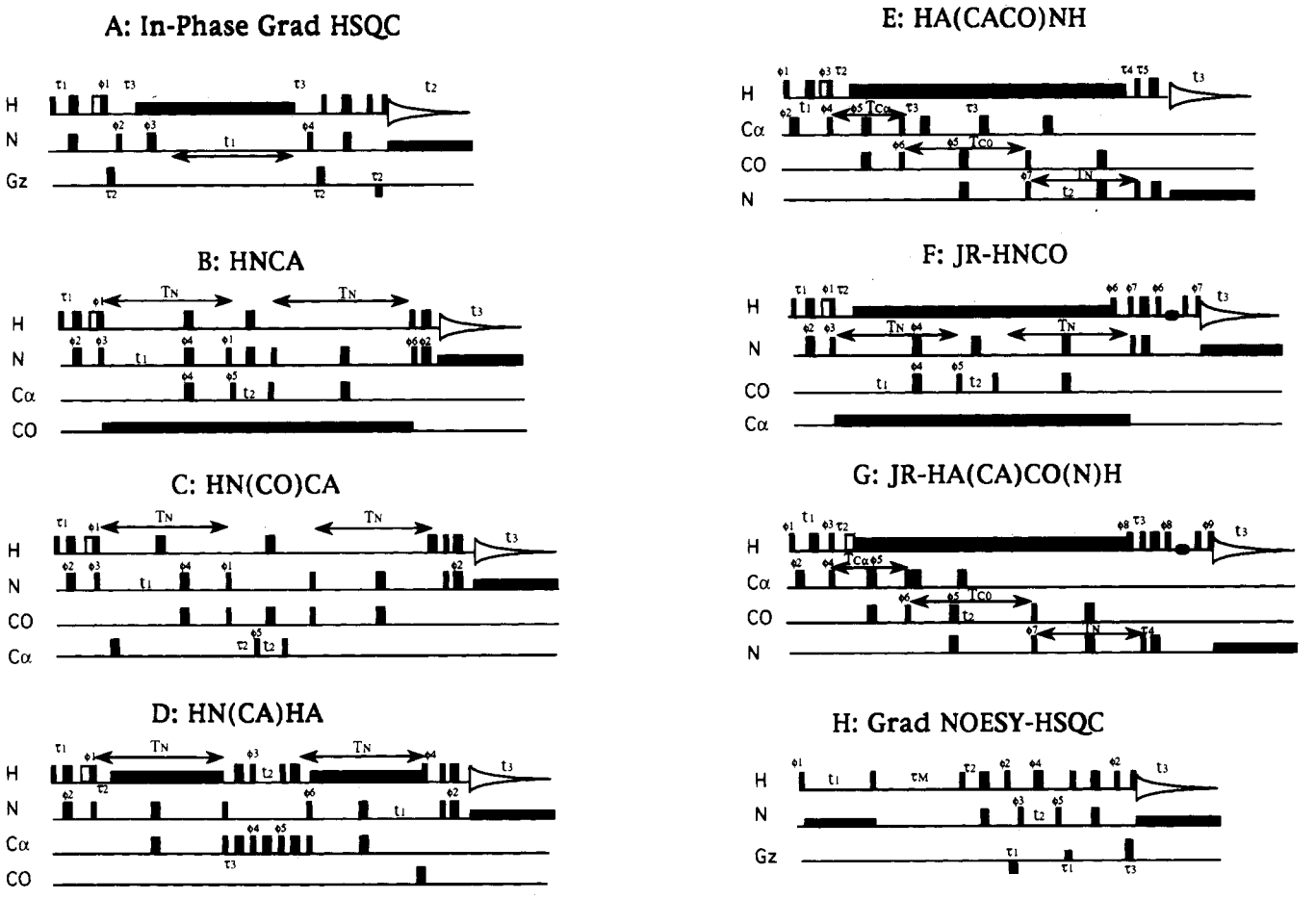

FIGURE 1: Pulse schemes of the experiments used in this investigation. Experimental conditions and parameters are described in the text. Narrow blocks represent 90° pulses, wider blocks 180° pulses. Long, black boxes identify decoupling sequences; open boxes denote full-power spin-lock purge pulses. The filled ellipsoids in panels F and G are homospoil pulses.

HN(CA)HA, 3D CT-HA(CACO)NH, jump-return 3D CT-HNCO, jump–return 3D CT-HA(CA)CO(N)H, and gradient-enhanced 3D ^{15}N-resolved NOESY-HSQC experiments used are shown in Figure 1A–G. The application of the experiments is given in the Results and Discussion section. Water suppression in all experiments shown included a 1-ms spin-lock pulse (Messerle et al., 1989). Weak preirridiation of water with an rf field strength of 4–7 Hz was also used in experiments B–E of Figure 1. Relaxation delays were 0.92–1.0 s. Waltz-16 decoupling (Shaka et al., 1983) of ^{15}N (1.4-kHz rf field strength) was applied during detection of amide protons in all experiments. The composite pulse decoupling of ^{1}H in the experiments shown in Figure 1A and Figure 1D-G was MLEV-16 (Levitt & Freeman, 1981) with an rf field strength of 4.3 kHz. The carrier positions (ppm) were 4.72 (^{1}H), 119.2 (^{15}N), 55.8 (^{13}C$^{\alpha}$), and 176.4 (^{13}CO) unless mentioned otherwise below. The 180° pulses on ^{15}N during INEPT and rev-INEPT transfers between amide protons and nitrogens were composite for the experiments shown in Figure 1B–D,G which were performed with 5-mm probes. In these composite pulses (for B–D), the phase of the flanking 90° pulses was ϕ_1. States-TPPI quadrature detection (Marion et al., 1989b) was used in all indirect dimensions.

The parameters for the new 2D ^{15}N gradient-enhanced, in-phase HSQC experiment (Figure 1A) were for t_1 and t_2, respectively: spectral width (ppm), 49.3, 18.2; number of acquired complex points, 512, 1024; digital resolution in processed data (Hz/pt), 2.4, 4.4. Delays (ms) were as follows: τ_1, 2.3; τ_2, 2.0; τ_3, 5.4. Rf field strengths (kHz) were 22.3 (^{1}H) and 6.6 (^{15}N). The gradient pulses (G/cm) were 12, 12, and –6, respectively. The phase cycle was as follows: $\phi_1 = 4(y), 4(-y)$; $\phi_2 = x, -x$; $\phi_3 = 8(x), 8(y), 8(-x), 8(-y)$; $\phi_4 = 2(x), 2(-x)$; receiver = $x, -x, -x, x, 2(-x, x, x, -x), x, -x, -x, x$. The quadrature was applied to ϕ_2. Total experimental time was 11 h, with 32 scans per matrix element. Relaxation of in-phase ^{15}N magnetization is slower than that of the antiphase magnetization present in conventional HSQC spectra (Peng & Wagner, 1992). Therefore, the in-phase experiment is expected to have superior resolution in the ^{15}N dimension.

The parameters for the 3D CT-HNCA experiment (Grzesiek & Bax, 1992; Figure 1B) were for t_1, t_2,and t_3, respectively: spectral width (ppm), 28.8, 31.9, 18.1; number of acquired complex points, 38, 48, 512; digital resolution in processed data (Hz/pt), 13.7, 18.8, 10.6. The ^{13}C$^{\alpha}$ carrier was placed at 54.7 ppm. Delays (ms): τ_1, 2.3; T_N, 22.1. The rf field strengths (kHz) were 13.5 (^{1}H), 7.8 (^{15}N), and 4.5 (^{13}C$^{\alpha}$). The ^{13}CO Waltz-16 decoupling was carried out with a 0.33-kHz field, in order to avoid measurable Bloch–Siegert shifts. The phase cycle was as follows: $\phi_1 = y, -y$; $\phi_2 = x, -x$; $\phi_3 = x$; $\phi_4 = 4(x), 4(y), 4(-x), 4(y)$; $\phi_5 = 2(x), 2(-x)$; $\phi_6 = y$; receiver = $2(x), 4(-x), 2(x)$. The States-TPPI quadrature was applied to ϕ_3 and ϕ_5. Total experimental time was 6 days with 64 scans per indirect quadrature element. To improve the sensitivity of the CT-HNCA and CT-HN-(CO)CA, one now utilizes in-phase ^{15}N magnetization (Peng & Wagner, 1992; Grzesiek & Bax, 1992) by performing composite-pulse ^{1}H decoupling as shown for other experiments in Figure 1.

The parameters for the 3D CT-HN(CO)CA experiment (Grzesiek & Bax, 1992; Figure 1C) were for t_1, t_2, and t_3, respectively: spectral width (ppm), 28.8, 29.2, 18.1; number

of complex points, 32, 48, 512; digital resolution in processed data (Hz/pt), 13.7, 17.2, 10.6. Delays (ms) were as follows: τ_1, 2.3; T_N, 20.2; τ_2, 8.3. The rf field strengths (kHz) were 13.5 (^{1}H), 7.8 (^{15}N), 4.6 (^{13}CO), and 4.5 ($^{13}C_\alpha$). The phase cycling was the same as for the CT-HNCA above. Total experiment time was 7.5 days with 96 scans per indirect quadrature element.

The HN(CA)HA experiment was essentially the revision of Olejniczak et al. (1992b) of the experiment of Clubb et al. (1992a) to include the in-phase ^{15}N coherence. For SCD this gave rise to a 50% increase in sensitivity. The parameters for the 3D CT-HN(CA)HA experiment (Figure 1D) were for t_1, t_2, and t_3, respectively: spectral width (ppm), 29.9, 4.0, 18.1; number of complex points: 20, 30, 512; digital resolution in processed data (Hz/pt), 14.2, 9.5, 10.6. Delays (ms) were as follows: τ_1, 2.3; τ_2, 5.5; T_N, 24.1; τ_3, 1.5. The rf field strengths (kHz) were 13.7 (^{1}H), 7.7 (^{15}N), 4.4 ($^{13}C_\alpha$), and 4.4 kHz (^{13}CO). The phase cycle was as follows: $\phi_1 = y, -y$; $\phi_2 = x, -x$; $\phi_3 = 2(x), 2(-x)$; $\phi_4 = y$; $\phi_5 = 4(y), 4(-y)$; $\phi_6 = 8(x), 8(-x)$; receiver = $x, -x, -x, x, 2(-x, x, x, -x), x, -x, -x, x$. The States-TPPI was applied to ϕ_3 and ϕ_6. Total experiment time was 7.5 days with 240 scans per indirect quadrature element.

The parameters for the 3D CT-HA(CACO)NH experiment (Boucher et al., 1992; Figure 1E) were for t_1, t_2, and t_3, respectively: spectral width (ppm), 3.5, 29.9, 18.1; number of acquired complex points, 40, 26, 512; digital resolution in processed data (Hz/pt), 8.2, 14.2, 10.6. A semi-constant-time period (Grzesiek & Bax, 1993) was employed during t_1. The initial duration of t_1 including pulse durations was 3.25 ms. Delays (ms) were as follows: τ_2, 3.5; $T_{C\alpha}$, 7.7; T_{CO}, 25.35; τ_3, 8.5; T_N, 25.1; τ_4, 5.4; τ_5, 2.25. The experiment was also modified by inclusion of a Bloch–Siegert compensation pulse (Grzesiek & Bax, 1993) on $^{13}C_\alpha$ during T_{CO}. The rf field strengths (kHz) were 18.2 (^{1}H), 4.8 (^{15}N), 4.5 ($^{13}C_\alpha$), and 4.3 (^{13}CO). The phase cycle was as follows: $\phi_1 = x$; $\phi_2 = x, -x$; $\phi_3 = 4(y), 4(-y)$; $\phi_4 = 8(x), 8(-x)$; $\phi_5 = 2(x), 2(y), 2(-x), 2(-y)$; $\phi_6 = 2(x), 2(-x)$; $\phi 7 = x, -x$; receiver = $x, -x, -x, x, 2(-x, x, x, -x), x, -x, -x, x$. The States-TPPI was applied to ϕ_1 and ϕ_7. Total experiment time was 2.7 days using 48 scans per indirect quadrature element.

The parameters for the 3D jump–return CT-HNCO experiment (Grzesiek & Bax, 1992; Figure 1F) were for t_1, t_2, and t_3, respectively: spectral width (ppm), 17.25, 29.9, 18.1; number of acquired complex points, 64, 40, 512; digital resolution in processed data (Hz/pt), 10.2, 14.2, 10.6. Instead of presaturation, a 5-ms homospoil gradient was applied during a z-filter, followed by a 15-ms recovery delay, followed by a jump–return. Rf field strengths (kHz) were 18.0 (^{1}H), 4.8 (^{15}N), and 4.6 (^{13}CO). Waltz-16 decoupling of $^{13}C_\alpha$ of only 330 Hz was applied to avoid Bloch–Siegert shifts of the ^{13}CO resonances at the cost of inadequate decoupling $^{13}C_\alpha$ resonances which lie at the edge of the $^{13}C_\alpha$ region, as occurs for glycines, valines, and threonines. The phase cycle was as follows: $\phi_1 = y, -y$; $\phi_2 = x, -x$; $\phi_3 = 4(x), 4(-x)$; $\phi_4 = 8(x), 8(-x)$; $\phi_5 = 2(x), 2(-x)$; $\phi_6 = y$; $\phi_7 = -x$; receiver = $x, -x, -x, x, -x, x, x, -x$. The quadrature was applied to ϕ_3 and ϕ_5. Using 16 scans per indirect quadrature element, total experiment time was 2 days.

The parameters of the 3D jump–return HA(CA)CO(N)H, a modification of the experiment of Boucher et al. (1992) shown in Figure 1G, were for t_1, t_2, and t_3, respectively: spectral width (ppm), 3.5, 17.25, 18.1; number of acquired complex points, 40, 50, 512; digital resolution in processed data (Hz/pt), 8.2, 20.3, 10.6. Rather than presaturation, a z-filter with a 10-ms homospoil pulse and 16-ms recovery period followed by a jump–return was used for water suppression. The t_1 period was incremented in a semi-constant time (Grzesiek & Bax, 1993). Delays (ms) were as follows: τ_2, 2.3; $T_{C\alpha}$, 7.7; T_{CO}, 27.8; T_N, 24.1; τ_3, 5.4; τ_4, 2.25. The delay τ_2 of 2.3 ms was a compromise in transfer of magnetization both from pairs of glycine α-protons and from single non-glycine α-protons. The rf field strengths (kHz) were 18.0 (^{1}H), 4.8 (^{15}N), 4.6 ($^{13}C_\alpha$), and 4.5 (^{13}CO). The phase tables are identical to those of the HA(CACO)NH with the addition of $\phi_8 = y$ and $\phi_9 = -x$. The quadrature was applied to ϕ_1 and ϕ_6. Total measuring time was 3.5 days using 32 scans per indirect quadrature element.

The parameters for the gradient-enhanced 3D NOESY-HSQC [cf. Majumdar and Zuiderweg (1993) and Figure 1H] were for t_1, t_2, and t_3, respectively: spectral width (ppm), 15.1, 29.6, 18.2; number of complex points acquired, 128, 48, 1024; digital resolution in processed data (Hz/pt), 14.8, 11.7, 8.9. The ^{15}N carrier was placed at 120.2 ppm. Delays (ms) were: τ_1, 1.1; τ_m, 70.0; τ_2, 2.3; τ_3, 4.1. Gradient strengths (G/cm) were 6, –6, and 18, respectively. Rf field strengths (kHz) were 22.3 (^{1}H) and 6.6 (^{15}N). The phase cycle was as follows: $\phi_1 = 4(x), 4(-x)$; $\phi_2 = y$; $\phi_3 = x, -x$; $\phi_4 = 8(x), 8(-x)$; $\phi_5 = 2(x), 2(-x)$; receiver = $x, -x, -x, x, -x, x, x, -x$. The quadrature was applied to ϕ_1 and ϕ_4. Acquisition time was 4.7 days using 16 scans per indirect quadrature element.

Processing of spectra was performed on a Silicon Graphics Indigo using Felix 2.0 (Hare Research, Inc.) with some modifications in reading, base-line correction, and complex linear prediction. The linear prediction routine was a gift of Dr. Mark Friedrichs. The constant-time ^{15}N labeling periods of experiments B–G were extended by 75% using "mirror-image" linear prediction (Zhu & Bax, 1990). Typically, squared cosine bell or Kaiser window functions were used in indirect dimensions. ^{15}N chemical shifts were referenced using ammonium nitrate (Levy & Lichter, 1979). ^{13}C chemical shifts were referenced against DSS. Peak picking was performed with Felix 2.05. Software was written to suggest potential neighbors in sequence by interpreting peak picks of the HNCA and HN(CO)CA experiments and to suggest neighbors in sequence by identifying symmetric d_{NN} NOEs from a peak pick of the amide region of ^{15}N-edited NOESY experiments. An interface for Felix for rapid display of multiple planes of different 3D spectra, written by Dr. Ananya Majumdar, further accelerated spectral interpretation. The interface, "Felixtalk", does not require Felix source code as it writes macros read by Felix.

RESULTS AND DISCUSSION

Sample Stability. Conditions have been found for which the catalytic fragment of human stromelysin-1 is very stable, qualifying it for long-term three- and four-dimensional NMR experiments. The activity of the SCD prepared from the insoluble fraction, the method of preparation used in this study, is equivalent to that prepared from the soluble fraction (Ye et al., 1992). Consistent with this observation, NOESY spectra of SCD purified from the insoluble and soluble fractions show no significant differences (not shown). SDS–PAGE analysis has shown degradation to lower molecular weight products accompanying loss of activity. The presence of Ca^{2+} ion stabilizes SCD, preventing autolytic degradation (Ye et al., 1992), just as others have found for a collagenase catalytic fragment (Lowry, 1992). The interaction between Ca^{2+} and MMPs is weak since millimolar concentrations are needed. In the bacterial zinc endoproteinase thermolysin, X-ray

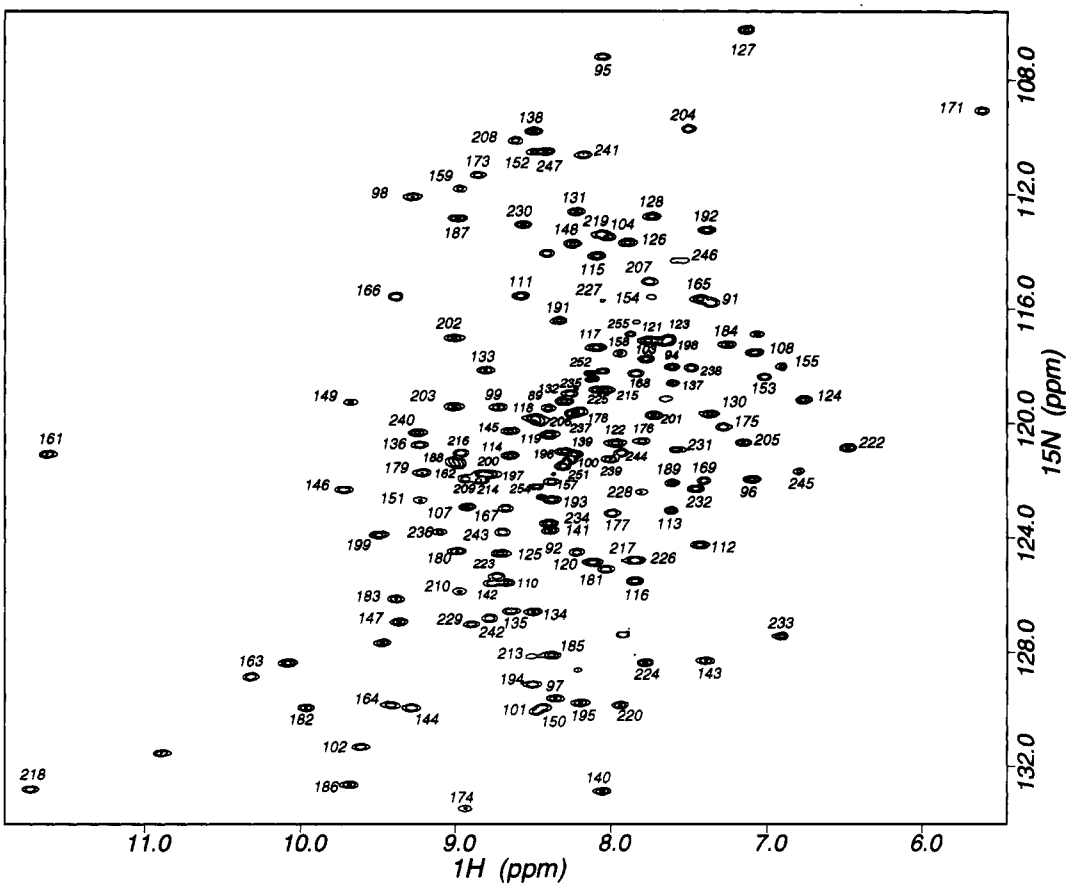

FIGURE 2: Gradient-enhanced, in-phase ^{15}N-HSQC spectrum at 11.7 T (Figure 1A) of 1.5 mM ^{15}N-labeled stromelysin catalytic domain (SCD), 10 mM deuterated Tris-HCl (pH 7.0), 20 mM $CaCl_2$, 15% acetonitrile-d_3, 8% D_2O, and 2 mM unlabeled hydroxamate inhibitor, U24522, 32 °C. The assigned peaks (exclusively backbone correlations in this experiment) are indicated by numbers (for sequence information, see Figure 6).

crystallography showed the requisite Ca^{2+} ions to be bound by carboxylate groups at the protein surface (Holmes et al., 1982). SCD is most stable at pH 7–8 and becomes more labile as the pH is decreased. SCD was shown to withstand incubation at 37 °C for 20 days at pH 7.0 or 8.0 with minimal loss of activity (Ye et al., 1992). However, the same incubation at pH 6.0 caused loss of more than half of its activity while incubation at pH 5.0 caused loss of more than half of activity in only 3 h. Consistent with this loss of stability, we have observed upon decreasing the pH from 7.0 to 6.0 (5 mM Ca^{2+}) the dramatic development of narrow amide lines at random coil chemical shifts, in HSQC spectra. This is suggestive of the segmental motion of denaturation occurring because of mild acidity with insufficient Ca^{2+} present. At the chosen conditions of pH 7.0 at 32 °C with 20 mM $CaCl_2$ and hydroxamate-substituted peptide inhibitor present, SCD has been stable and free of denaturation for several months as judged from ^{15}N-HSQC spectra (cf. Figure 2) and HSQC projections of triple-resonance spectra. A drawback of the "high" pH of 7.0 is that amide proton exchange rates are relatively high, which decreases spectral quality for certain regions of SCD as described below.

Sample Aggregation. Given its stability and its molecular size of 174 amino acid residues (19.5 kDa for unlabeled sample, see Figure 6 for sequence information), the determination of the solution structure of the catalytic domain of stromelysin-1 should be well within range of the modern multinuclear three- and four-dimensional NMR techniques (Fesik & Zuiderweg, 1988, 1990; Marion et al., 1989a; Clore & Gronenborn, 1990; Ikura et al., 1990, 1992). NOESY, HOHAHA, and HSQC spectra display favorable chemical shift dispersion but suggested formation of soluble aggregates at concentrations above 0.5 mM, manifest by ^{1}H line widths averaging 34 Hz and ^{15}N line widths averaging 17 Hz at 1.1 mM at room temperature. The aliphatic carbon resonances of ^{15}N/^{13}C-labeled material under similar conditions at 1.7 mM averaged 50 Hz or higher. These line width parameters make most experiments but the ^{15}N-resolved NOESY spectra unacceptably low in sensitivity. Using 15% acetonitrile in the buffer, the molecule gives rise to 20–25-Hz amide proton lines and 7-Hz (^{1}H decoupled) ^{15}N lines, at 32 °C, suggesting that the polar organic cosolvent shifts the aggregation toward the monomeric state. The improvement in line widths brings about a dramatic improvement in the efficiency of triple-resonance experiments. The addition of acetonitrile to the sample did not cause denaturation and did not affect other NMR parameters apart from small changes in amide chemical shifts, as judged by comparisons using ^{15}N-HSQC and ^{15}N-edited NOESY spectra. The one unfavorable property of addition of acetonitrile is to limit solubility of SCD to about 1.5 mM.

Assignment of the Main-Chain Resonances. The HOHAHA experiment on SCD yielded NH–Hα cross peaks for only about 45% of the residues and few transfers to β-protons or beyond for any residue, except for four residues which turned out to be the last four non-proline residues of SCD (not shown). The ^{15}N-resolved NOESY-HSQC/HOHAHA-HSQC assignment method (Fesik & Zuiderweg, 1990; Marion et al., 1989a) that has been successfully applied to a number of larger proteins [e.g., Stockman et al. (1992)] could therefore not be used, and triple-resonance assignment methods with ^{13}C/^{15}N doubly labeled material (Ikura et al., 1990) had to be followed. The broad line widths, even in the presence of

acetonitrile, restricted the choice of triple-resonance experiments to only the most sensitive ones. Figure 2 shows the ^{15}N-HSQC spectrum of SCD. This spectrum is well resolved, promising that the triple-resonance experiments, most of which rely on this "fingerprint" for two of their dimensions, will be resolved at least as well. The spectrum in Figure 2 was recorded with in-phase ^{15}N single-quantum coherence and was tuned to suppress the NH_2 resonances of the glutamine and asparagine sidechains (see Figure 1A). The assignments as obtained here are indicated in the figure. The figure clearly shows that the assignment is virtually complete, as is also more readily found from Figure 6 and Table I. Three strong cross peaks lacking assignment, located at the {^{1}H,^{15}N} coordinates {10.9, 131.8}, {10.1, 128.2}, and {9.5, 128.0}, likely arise from the indole groups of the three tryptophan residues.

The assignment strategy was as follows:

(1) The 3D CT-HNCA and 3D-CT-HN(CO)CA experiments were used to obtain the chemical shift correlation between HN(i), N(i), $C_\alpha(i)$ and $C_\alpha(i-1)$ for each amino acid, thus forming "T"-like connections. "T's" were constructed automatically, using software written to interpret peak picks of the HN(CO)CA and HNCA experiments. This was successful for 80% of the residues on the basis of the well-resolved ^{15}N–^{1}H spectrum. "T's" were not automatically constructed for 20% of the residues including (i) the several prolines, (ii) those with amide proton signals attenuated by magnetization transfer from presaturated water, or (iii) those with overlapping peaks in the ^{15}N–^{1}H spectrum. Where this overlap of amides occurs, an additional 6% of the T's were constructed manually, i.e., for the overlapping pairs A200/N214, E118/S206, I101/E150, R100/E139, and A217/L226. The software linked the Ts to probable neighboring Ts via matching $^{13}C\alpha$ frequencies. Typically, four or five T's were candidates for the genuine neighbor. Therefore, another assignment path was needed to discriminate among the candidates.

(2) To narrow the possibilities, the $^1H_\alpha$ path was used in addition to the $^{13}C_\alpha$ path. A process similar to that described above was carried out, constructing T's for the HN(i), N(i), $H_\alpha(i)$ and $H_\alpha(i-1)$ resonances of every peptide linkage, using the 3D CT-HN(CA)HA and 3D HA(CACO)HN experiments (Figure 1C,D). The $H_\alpha(i-1)$–N(i)H(i)–$H_\alpha(i)$ "T's" could be successfully constructed for 80% of the residues. The number of T's was slightly lower than for the C_α T's because the H_α experiments were tuned to totally suppress the resonances of glycines. Subsequently, the H_α frequencies of the obtained "T's" were compared with each other and matched.

(3) The lists of possible connections via the $H_\alpha(i-1)$N(i)H(i)$H_\alpha(i)$ and $C_\alpha(i-1)$N(i)H(i)$C_\alpha(i)$ T's were compared to select the connections common to both lists. This comparison gave rise to many stretches of connected T's, verified by visual inspection. Figure 3 shows such an alignment of the results from the 3D HNCA, HN(CO)CA, HN(CA)HA, and HA(CACO)NH experiments for the assignment of several of the main-chain resonances of SCD. In the top of the figure, alternating (^{1}H,$^{13}C_\alpha$) planes of HNCA and HN(CO)CA at fixed ^{15}N frequencies are shown. The HNCA/HN(CO)CA pairs identify the trans-peptide $C_\alpha(i-1)$N(i)H(i)$C_\alpha(i)$ T's. The bottom half of the figure shows a similar construction for the $H_\alpha(i-1)$N(i)H(i)H_α(i) T's and their connections. The HNCA experiment gives rise both to the *intra*residue HN$C\alpha$ correlation (over a one bond ^{15}N to $^{13}C\alpha$ coupling) and to a usually weaker *inter*-residue HN(i)$C_\alpha(i-1)$ correlation (over a weaker two-bond coupling) (Kay et al., 1990). Because the interresidue correlation is not always clearly weaker as seen in the strips for G176 and D181 of Figure 3, it is better to identify the interresidue (trans-peptide) connectivity from the HN(CO)CA experiment. Whereas the trans-peptide link is a single shared C_α frequency, the HNCA and HN(CO)CA peaks are tied together through two shared frequencies, that of the amide proton and nitrogen chemical shifts. These connections are implicit in this figure. The HN(CA)HA experiment can also give rise to two peaks for every amino acid over the same couplings, but the delays in this experiment were set to diminish the interresidue (i–1) correlation (Clubb et al.,1992a). Some of the situations encountered in the assignment process using the C_α and H_α pathways are illustrated in Figure 3. The stretch from N175 to W186 (Figure 3) encompasses β-strand V. In this stretch, near degeneracy of sequential C_α shifts complicates connection of A178 with H179; of D181 with D182; and of E184 with Q185. In these three cases, the presence of the i–1 correlation in the HNCA is hidden by overlap but revealed by comparison with HN(CO)CA peaks. Well-resolved H_α connections provide an independent path to establish these particular connections muddled by the C_α overlap. A limitation of the H_α pathway is seen in that correlations to pairs of glycine α-protons are absent from both HA(CACO)NH of D177 and HN(CA)-HA of G176. As described previously (Boucher et al., 1992; Olejniczak et al., 1992b), this occurs because the experiments are tuned for optimal transfer of magnetization to single α-protons, sacrificing any transfer to the pairs of α-protons of glycine residues. Though partial degeneracy occurs for F180 and D181, the $^{13}C_\alpha$ path establishes this connection.

(4) Conventional NOESY-based paths of assignment confirmed connections from the two triple-resonance paths. The HN(CA)HA and HA(CACO)NH experiments were used to differentiate intraresidue from interresidue NH–H_α NOEs, respectively, in the ^{15}N-resolved NOESY spectrum (Figure 1G). This made the ^{15}N-resolved NOESY spectrum usable for classical $d_{\alpha N}$ NOE tracing. Figure 4A shows two interleaved stretches of sequential alignments in the 3D NOESY-HSQC spectrum belonging to β-strands I and II at one end of the β-sheet (cf. Figure 8). The sequential $d_{\alpha N}$ NOEs lie at the right-hand vertices of the thin horizontal lines connecting the "skewers" of neighboring residues *within* a strand. The intraresidue NOEs lie at the left-hand vertices of the thin horizontal lines. Several cross-sheet $d_{\alpha N(i,j)}$ NOEs (thick lines) delineating parallel β-sheet secondary structure are also illustrated in Figure 4A. The connectivities illustrated are also shown in the topology diagram (Figure 6).

(5) For those residues in helices, the pathway of amide–amide NOEs was also available. It does not depend upon the through-bond correlations obtained from the triple-resonance experiments, except for determining the directionality of a connection. The peaks of the amide region of the 3D NOESY-HSQC spectrum were picked. Software searched this list for the symmetric amide–amide NOEs indicative of "skewers" neighboring in sequence. Usually only one potential neighbor for any given d_{NN} NOE was found by this procedure. Figure 4B shows a consecutive stretch of such d_{NN} NOEs, identified from the 3D NOESY-HSQC spectrum in the active-site helix (helix B; cf. Figure 6) in SCD. Figure 4B shows also some $d_{\alpha N(i,i+3)}$ and $d_{\alpha N(i,i+4)}$ NOEs establishing the helicity of this region of the protein.

(6) The connected fragments were placed in the amino acid sequence using a combination of methods:

(a) Three specifically ^{15}N-labeled samples were prepared: [^{15}N]Leu-SCD, [^{15}N]Ala-SCD, and [^{15}N]Phe-SCD. The

Table I: Main-Chain Chemical Shifts for Human Stromelysin Catalytic Domain[a]

residue	^{1}H(N)	^{15}N	^{13}CO	$^{13}C_\alpha$	$^1H_\alpha$	residue	^{1}H(N)	^{15}N	^{13}CO	$^{13}C_\alpha$	$^1H_\alpha$
Gly 88			173.2	45.0		Asn 162	9.01	121.3	174.5	56.5	4.17
Ile 89	8.44	119.5		60.4		Val 163	10.30	128.8	178.6	65.6	4.05
Pro 90			176.2	63.3	4.39	Leu 164	9.41	129.8	175.8	56.1	4.68
Lys 91	7.38	115.7	175.4	54.6	4.50	Ala 165	7.42	115.5	176.0	51.8	4.53
Trp 92	8.23	124.5		57.8	4.58	His 166	9.39	115.5	172.1	54.2	5.01
Arg 93			174.8	55.2	4.65	Ala 167	8.69	122.9	174.5	51.4	5.05
Lys 94	7.61	118.1	174.3	54.2	4.82	Tyr 168	7.85	118.3	173.9	56.6	4.34
Thr 95	8.08	107.1	172.6	61.2	4.36	Ala 169	7.45	121.9		50.2	4.05
His 96	7.10	121.8	173.9	54.1	5.14	Pro 170			174.4	64.2	3.10
Leu 97	8.35	129.7	176.4	52.8	4.54	Gly 171	5.61	109.1		43.9	4.04
Thr 98	9.27	111.9	174.6	58.1	5.84	Pro 172			177.7	62.7	4.75
Tyr 99	8.72	119.3	171.8	54.7	5.74	Gly 173	8.88	111.3	175.3	46.7	3.94
Arg 100	8.26	121.3	174.0	55.0	4.41	Ile 174	8.98	133.5	174.3	61.9	4.26
Ile 101	8.47	129.8	175.5	61.5	4.39	Asn 175	7.27	120.1	175.6	55.9	4.26
Val 102	9.63	131.4	175.3	65.9	3.48	Gly 176	7.79	120.4	171.7	45.7	4.57, 4.10
Asn 103	7.78	117.7	169.9	51.1	4.76	Asp 177	8.00	123.1	173.9	55.4	4.74
Tyr 104	8.04	113.4		58.6	4.34	Ala 178	8.19	119.5	174.9	51.1	5.01
Thr 105						His 179	9.21	121.7	173.4	50.8	5.87
Pro 106			177.3	63.1	4.66	Phe 180	8.99	124.5	174.0	56.7	4.34
Asp 107	8.93	122.9	175.4	55.8	4.16	Asp 181	8.03	125.0	179.3	53.8	4.40
Leu 108	7.07	117.5		51.0	4.96	Asp 182	9.96	129.9	179.3	53.2	5.60
Pro 109			177.8	62.2	4.57	Asp 183	9.38	126.0	177.2	56.4	5.01
Lys 110	8.71	125.5	178.2	60.4	3.80	Glu 184	7.25	117.3	175.9	53.2	4.55
Asp 111	8.58	115.4	178.6	56.7	4.40	Gln 185	8.42	128.1	173.6	53.4	4.43
Ala 112	7.41	124.2	180.4	54.2	4.37	Trp 186	9.70	132.7	177.3	57.3	5.04
Val 113	7.60	123.1	177.1	66.3	3.60	Thr 187	9.00	112.7	175.5	60.1	4.98
Asp 114	8.65	121.1	178.8	58.0	4.25	Lys 188	9.05	121.2	176.0	56.5	4.62
Ser 115	8.10	114.1	176.4	61.4	4.29	Asp 189	7.58	122.1		52.4	4.97
Ala 116	7.82	125.4	179.3	55.7	4.21	Thr 190			174.9	61.8	4.71
Val 117	8.08	117.3	177.0	67.0	3.30	Thr 191	8.34	116.3	175.2	64.1	4.30
Glu 118	8.50	119.7	179.5	60.3	3.75	Gly 192	7.40	113.2	173.4	45.1	3.63, 4.31
Lys 119	8.42	120.4	178.6	59.5	4.00	Thr 193	8.41	122.8	173.2	62.2	3.83
Ala 120	8.14	124.9	178.1	55.7	4.02	Asn 194	8.51	129.2	175.1	55.4	4.97
Leu 121	7.77	117.0	179.7	57.7	3.74	Leu 195	8.17	129.7	176.5	58.1	4.55
Lys 122	7.94	120.6	178.7	58.4	4.18	Phe 196	8.34	121.1	175.2	61.1	4.10
Val 123	7.62	116.8	177.2	65.4	3.82	Leu 197	8.81	121.7	179.1	57.9	3.17
Trp 124	6.76	119.1	180.0	57.9	4.75	Val 198	7.65	117.2	178.7	66.6	3.74
Glu 125	8.71	124.5	178.4	59.6	4.01	Ala 199	9.52	123.9	178.4	56.0	4.09
Glu 126	7.91	113.4	177.9	58.7	4.20	Ala 200	8.84	121.7	179.8	56.6	3.99
Val 127	7.13	106.1	174.6	60.1	4.78	His 201	7.71	119.6	176.0	59.8	4.36
Thr 128	7.73	112.7		60.1	5.53	Glu 202	9.02	116.9	178.8	58.2	4.38
Pro 129			176.4	62.2	5.00	Ile 203	9.02	119.3	177.2	61.7	3.87
Leu 130	7.38	119.5	176.7	54.8	4.59	Gly 204	7.50	109.6	177.3	48.4	2.46, 4.09
Thr 131	8.25	112.3	172.5	59.9	4.59	His 205	7.14	120.5	178.8	57.3	5.68
Phe 132	8.33	118.9	177.0	56.1	5.84	Ser 206	8.47	119.9	175.7	62.7	4.80
Ser 133	8.79	118.0	171.4	57.7	4.97	Leu 207	7.75	114.8	178.5	55.2	4.63
Arg 134	8.53	126.5	175.6	55.5	3.61	Gly 208	8.62	110.0	173.4	44.9	3.52, 5.01
Leu 135	8.65	126.6	177.1	52.9	4.74	Leu 109	8.95	121.8	176.0	54.1	4.90
Tyr 136	9.27	120.6	174.1	58.7	4.45	Phe 210	8.99	125.9		54.0	4.10
Glu 137	7.59	118.4	174.7	54.5	4.45	His* 211	5.41	122.8			
Gly 138	8.55	109.7	172.4	44.3	3.82, 4.12	Ser 212			174.9	56.4	4.34
Glu 139	8.26	120.9	175.3	55.8	4.39	Ala 213	8.59	128.2	176.8	52.3	4.68
Ala 140	8.08	133.1	176.1	49.4	4.54	Asn 214	8.85	122.0	175.7	53.6	4.67
Asp 141	8.41	123.7	177.6	58.6	4.50	Thr 215	8.07	118.8	175.2	63.8	2.43
Ile 142	8.77	125.4	174.6	60.8	4.29	Glu 216	8.99	121.0	176.2	55.9	4.35
Met 143	7.39	128.2	177.0	53.8	5.01	Ala 217	7.86	124.9	51.8	4.63	
Ile 144	9.31	130.1	174.2	60.8	5.45	Leu 218	11.74	133.0	180.3	57.6	4.57
Ser 145	8.65	120.2	172.0	56.8	5.14	Met 219	8.07	113.3	177.1	53.1	4.82
Phe 146	9.73	122.1	176.0	56.7	5.32	Tyr 220	7.94	129.8		57.7	5.05
Ala 147	9.38	127.0	175.1	50.9	4.93	Pro 221			174.7	64.8	3.70
Val 148	8.28	113.6	174.4	59.5	4.98	Leu 222	6.47	120.8	175.5	53.1	5.05
Arg 149	9.67	119.0	177.5	56.5	3.87	Tyr 223	8.74	125.4	174.8	58.0	4.29
Glu 150	8.48	130.0	175.2	58.0	4.35	His 224	7.85	128.6	172.9	54.5	4.64
His 151	9.23	122.5	174.4	54.7	5.16	Ser 225	8.12	119.0	174.3	58.3	4.17
Gly 152	8.53	110.6	173.7	45.8	3.61, 4.19	Leu 226	7.85	124.8		54.2	4.63
Asp 153	7.02	118.4	175.3	51.0	4.59	Thr 227	8.07	115.6	174.3	63.8	4.20
Phe 154	7.81	115.5	173.9	58.5	4.33	Asp 228	7.84	122.3	176.9	52.9	4.83
Tyr 155	6.92	117.9		54.4	4.95	Leu 229	8.95	127.1	178.9	56.9	4.19
Pro 156				63.2	4.53	Thr 230	8.56	112.9	175.8	64.5	4.20
Phe 157	8.41	122.2	176.1	57.9	5.05	Arg 231	7.57	120.9	175.6	54.8	4.46
Asp 158	7.93	117.4	177.9	53.6	4.77	Phe 232	7.46	122.3	174.6	60.2	4.20
Gly 159	8.98	111.8		44.2	4.86	Arg 233	6.95	127.6	174.5	54.2	4.01
Pro 160				63.8	3.91	Leu 234	8.46	123.5	177.0	55.0	3.84
Gly 161	11.64	121.1	173.6	43.7	4.07, 3.24	Ser 235	8.26	119.0	175.4	58.3	4.53

Table I (Continued)

residue	$^1H(N)$	^{15}N	^{13}CO	$^{13}C_\alpha$	$^1H_\alpha$	residue	$^1H(N)$	^{15}N	^{13}CO	$^{13}C_\alpha$	$^1H_\alpha$
Gln 236	9.13	123.8	177.5	58.4	3.93	Tyr 246	7.54	114.1	175.7	58.7	4.87
Asp 237	8.28	119.6	177.9	58.7	4.58	Gly 247	8.44	110.5		44.2	
Asp 238	7.48	118.0	178.0	57.4	4.73	Pro 248					
Ile 239	8.00	121.3	177.6	65.7	3.64	Pro 249					
Asn 240	9.27	120.2	178.7	55.1	4.37	Pro 250			176.5	62.9	4.47
Gly 241	8.19	110.6	176.2	46.2		Asp 251	8.35	121.6	175.9	54.0	4.63
Ile 242	8.80	127.0	178.3	60.9	4.38	Ser 252	8.17	118.3		56.1	4.83
Gln 243	8.70	123.6	179.8	58.3	4.28	Pro 253			176.8	63.3	4.53
Ser 244	7.93	121.0	174.9	61.7	4.29	Gly 254	8.51	122.4	175.5	56.7	4.36
Leu 245	6.79	121.7	177.8	56.7	4.18	Thr 255	7.90	116.8		58.7	4.62

[a] Conditions were as follows: 0.6–1.5 mM SCD^{83-256}, 32 °C, pH 7.0, and 15% acetonitrile-d_3. Chemical shifts are reported in ppm relative to DSS (^1H and ^{13}C) and $^{15}NH_4{}^{15}NO_3$ (^{15}N; Levy & Lichter, 1979). *Assignments for this residue are tentative because of low signal intensities.

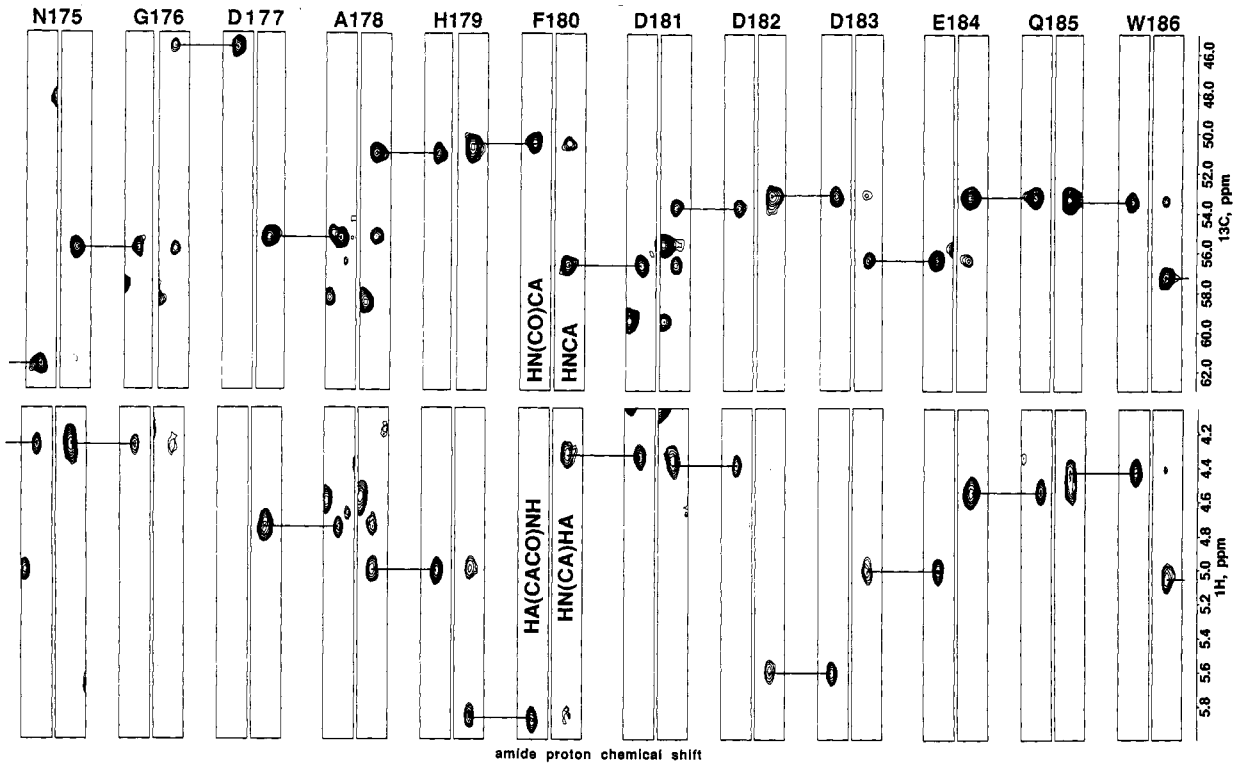

FIGURE 3: The alignment of the results from the 3D CT-HNCA, CT-HN(CO)CA, CT-HN(CA)HA, and CT-HA(CACO)NH experiments (Figure 1B–E) for the assignment of the main-chain resonances of N175–W186 of SCD. The sample was 1.4 mM $^{13}C/^{15}N$-labeled SCD for the CT-HNCA, CT-HN(CO)CA, and CT-HN(CA)HA experiments in a 5-mm probe and 0.6 mM $^{13}C/^{15}N$-labeled SCD for the CT-HA-(CACO)NH experiment in an 8-mm probe. The data were recorded at 14 T. Further experimental conditions are described in the text and the legend of Figure 2. In the top of this figure alternating (^1H,$^{13}C_\alpha$) planes of HNCA and HN(CO)CA at particular ^{15}N frequencies are shown as exemplified for F180. The ^{15}N planes and the amide proton shift ranges were taken at the frequencies corresponding to the residues shown at the top of the figure. The HNCA / HN(CO)CA pairs identify the trans-peptide $C_\alpha(i-1)N(i)H(i)C_\alpha(i)$ "T's". The "T's" are connected sequentially as indicated. The bottom half of this figure shows a similar construction for the $H_\alpha(i-1)N(i)H(i)H_\alpha(i)$ "T's" and their connections.

HSQC experiments of these samples gave residue type identification for 37 $^{15}N/^1H$ coordinate pairs as shown in Figure 5. The residues for labeling were chosen to produce the largest spread of known resonances (together with the glycine residues) in the sequence and for their position in the amino acid synthesis pathways of *E. coli*. Note that each HSQC spectrum shows exactly the number of cross peaks expected for the number of residues of that type in the protein but that Ala 213 is missing. To investigate the possibility that A213 was hidden by overlap, a gradient-enhanced NOESY-HSQC (Figure 1H) was collected for the [^{15}N]-alanine sample. No evidence was found for two overlapping alanine skewers. Rather, the amide of A213 is simply very weak (due to its relatively fast exchange with water evident by the presence of a strong water exchange peak in the gradient-enhanced NOESY-HSQC). The very weak amide of A213 can be seen in the gradient-enhanced HSQC at 1.5 mM (Figure 2), but the signal-to-noise ratio was too low for it to be seen at the 0.6 mM concentration of the [^{15}N]alanine sample (Figure 5). Leakage of the three labels into other residues was not detected even though the strain used was not aminotransferase-deficient as recommended by Muchmore et al. (1989). However, extensive leakage of the alanine and leucine labels was not expected since their transaminations are repressed by other amino acids present in the medium (Muchmore et al., 1989).

(b) The characteristic upfield chemical shifts of the ^{15}N and $^{13}C_\alpha$ resonances of the glycine residues (110 and 44 ppm, respectively) identified the $C_\alpha(i-1)N(i)H(i)C_\alpha(i)$ T's of these residues. The $^{13}C_\alpha$ frequencies are unique from other residues and are definitive. Figure 3B shows an example of the distinctive upfield $^{13}C_\alpha$ shift of a glycine (G176). The ^{15}N chemical shifts were somewhat less useful because they are not nearly so unique. The ^{15}N chemical shifts of G161 and

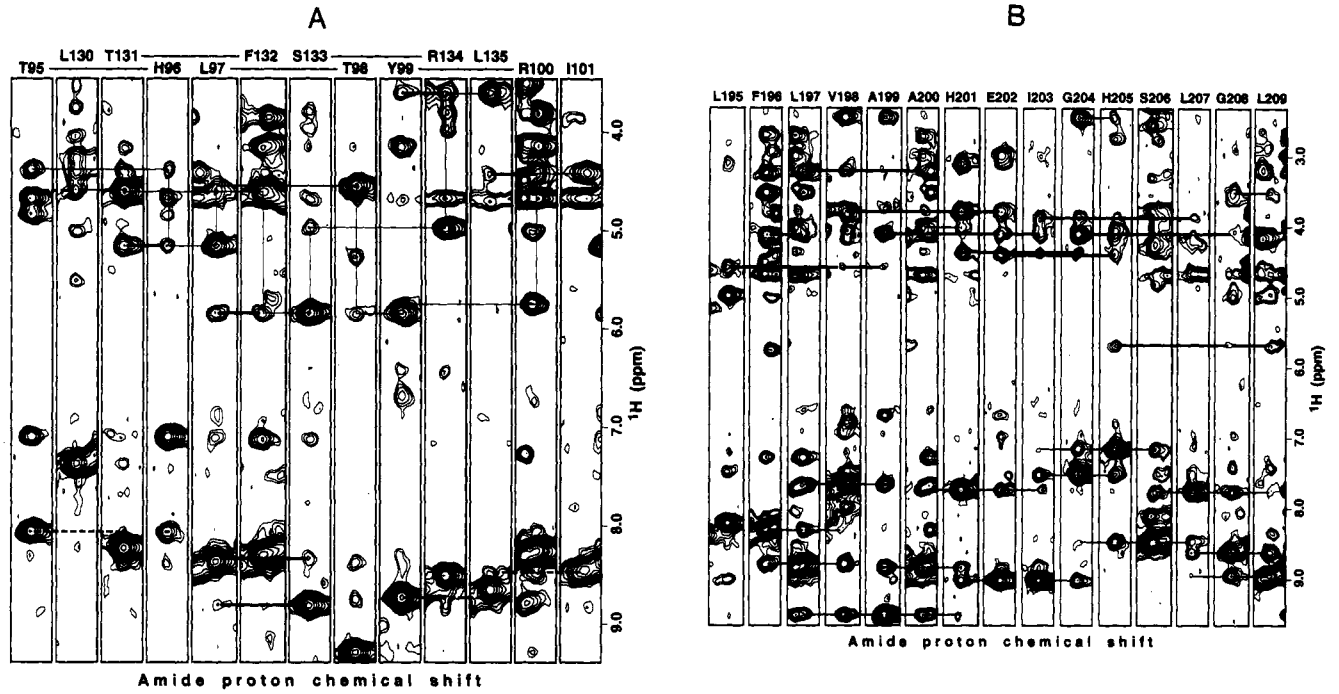

FIGURE 4: The alignment of the ^{1}H-amide "skewers" at the corresponding ^{15}N frequency from the 3D ^{15}N-resolved NOESY-HSQC spectrum at 11.7 T. The data were collected using pulsed-field gradient techniques (Figure 1G) with a 1.5 mM ^{15}N-labeled sample of SCD. Conditions were identical to those described with Figure 2. (A) Alignment of the residues forming strands I (95–101) and II (130–135) of the β-sheet presented in an interleaved manner to show sequential as well as interstrand NOEs. The sequential NOE connectivities are indicated for each strand, with continuous thin lines linking the intraresidue $d_{\alpha N(i,i)}$ NOEs and sequential $d_{\alpha N(i,i+1)}$ NOEs. Thick lines show interstrand NOEs, indicative of parallel β-sheet [$d_{\alpha N(i,j)}$]. Dashed lines indicate that the absence or presence of interstrand NOEs could not be established from the data. (B) The sequential alignment of the residues forming the active-site helix (residues L195–L209) of SCD. Sequential [$d_{NN(i,i\pm1)}$, $d_{NN(i,i\pm2)}$ and $d_{\alpha N(i,i+1)}$] NOEs are indicated with thin lines. Medium-range [$d_{\alpha N(i,i+3)}$ and $d_{\alpha N(i,i+4)}$] NOEs, indicative of helicity, are shown in thick lines.

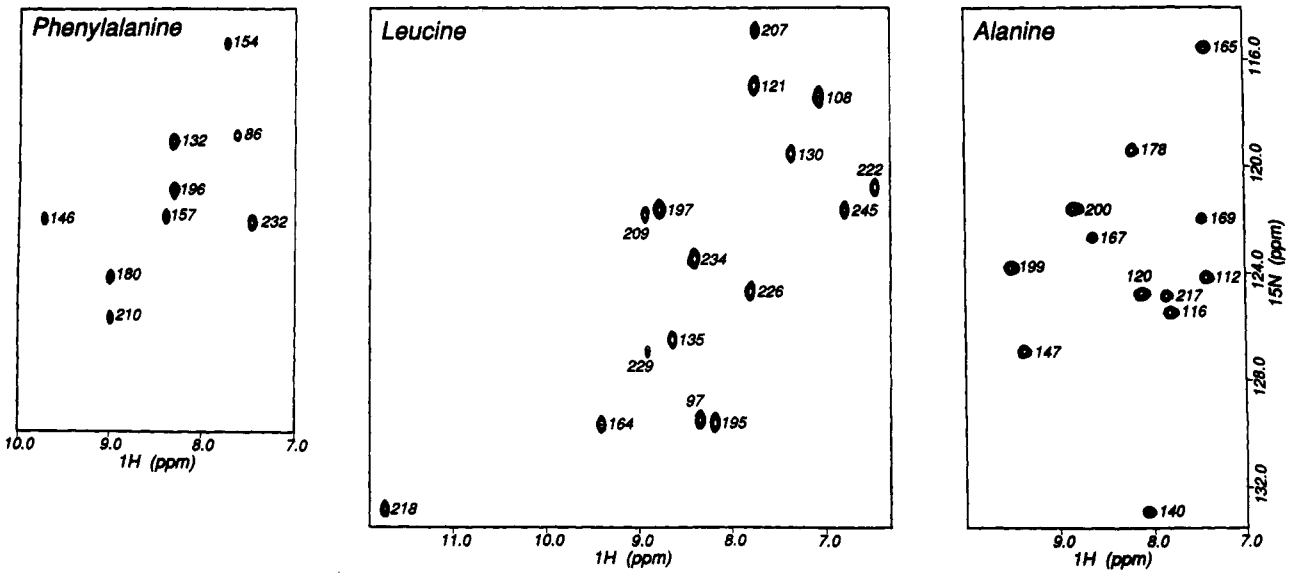

FIGURE 5: Gradient-enhanced ^{15}N-HSQC spectra of [^{15}N]Phe-SCD (left), [^{15}N]Leu-SCD (middle), and [^{15}N]Ala-SCD (right). Experimental conditions were similar to those described for Figure 2. Assignments are indicated in the figure. The assignment for Phe 86 is tentative.

G176 are unusually far downfield. The identifications were corroborated by the fact that the corresponding $H_\alpha(i-1)$N-(i)H$(i)H_\alpha(i)$ T connectivities were absent for these residues since the delays in the contributing HN(CA)HA and HA(CACO)HN experiments were tuned such that glycines would not yield peaks (see Figure 4). An additional experiment with modified tuning [HA(CA)CO(N)H of Figure 1G] allowing these signals to come through was recorded to further verify this negative evidence (see below).

(c) The HN(CA)HA and HA(CACO)NH experiments allowed a placement of the T fragments in the ^{15}N-resolved NOESY spectrum. The NOESY data were examined for patterns corresponding to specific pairs of adjacent residues to check placements of the fragments. This proved particularly useful for checking the identities of serine, threonine, and valine residues, that have quite distinctive ^{1}H NOE connectivity patterns. All NOESY skewers were checked for consistency with the assigned spin system type. Full side-chain assignments were obtained for the last four non-proline residues from a conventional TOCSY-HSQC (not shown), placing these spin sytems at the C-terminus.

(d) The extremely low-field $^{13}C_\alpha$ chemical shifts of valines and threonines were also helpful in placing connected stretches in the sequence. The many prolines, lacking amide protons

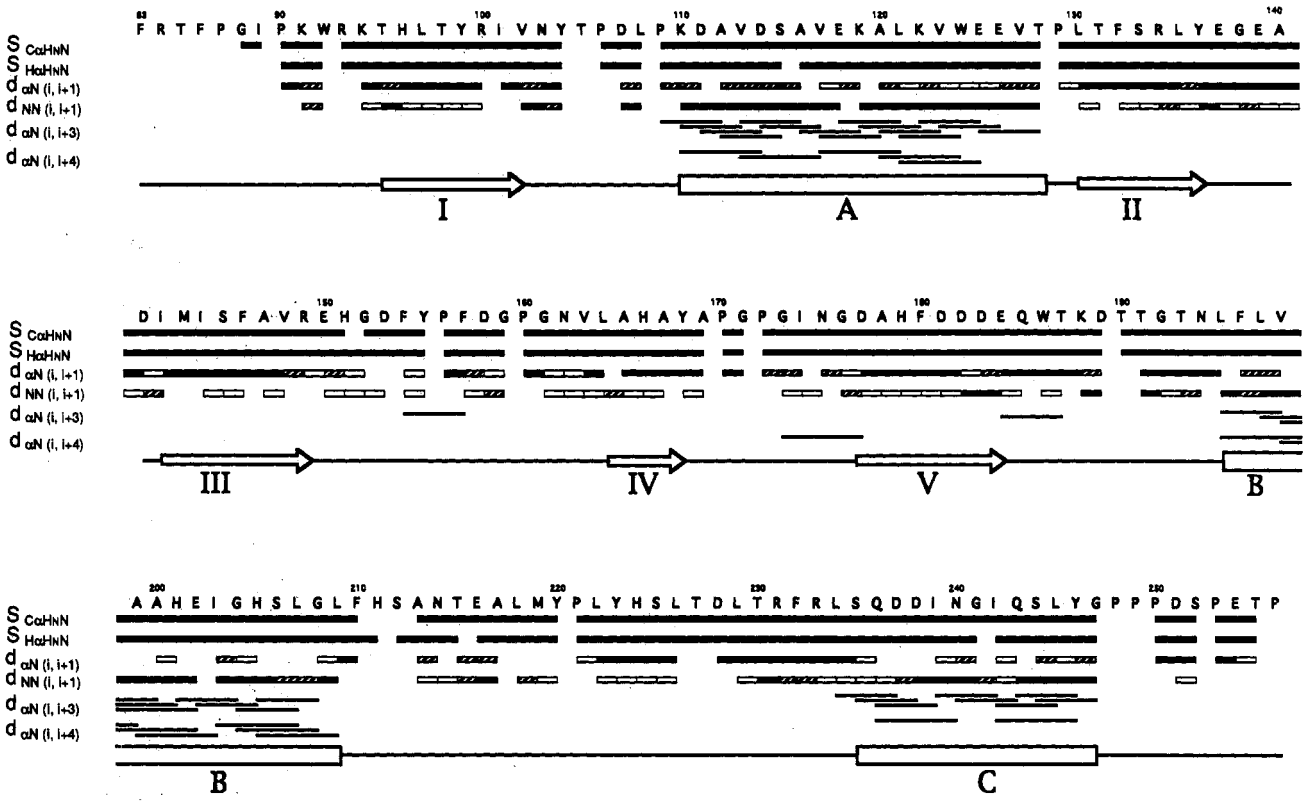

FIGURE 6: Sequence, assignment, and secondary structure for human stromelysin catalytic domain. Numbering starts with the first residue of the zymogen form of human stromelysin-1 lacking the signal sequence. $S_{C\alpha HNN}$ (S for scalar) are connectivities obtained from the C_α T's; $S_{H\alpha HNN}$ are those obtained from the H_α T's. The classical $d_{\alpha N(i,i+1)}$ and $d_{NN(i,i\pm1)}$ NOE connectivities (Wüthrich, 1986) were obtained from the 3D ^{15}N-resolved NOESY-HSQC spectrum. The first row labeled $S_{C\alpha HNN}$, shows the connections obtained by the pairing of the CT-HNCA and CT-HN(CO)CA experiments as exemplified in Figure 3. The second row, labeled $S_{H\alpha HNN}$, shows the connections obtained from the CT-HN(CA)HA and CT-HA(CACO)HN experiments. The third row is the $d_{\alpha N(i,i+1)}$ NOE connectivity, obtained from the 3D NOESY-HSQC data such as shown in Figure 4. Open boxes show weak cross peaks, hatched boxes show medium cross peaks, and black boxes show strong cross peaks. The absence of a connection indicates either true absence or possible overlap with other peaks. The fourth row is the $d_{NN(i,i\pm1)}$ NOE connectivity, obtained from the 3D NOESY-HSQC data as shown in Figure 4B. Open boxes show weak cross peaks, gray boxes show medium cross peaks, and black boxes show strong cross peaks. The absence of a connection indicates either true absence or possible overlap with other peaks. The fifth and sixth rows show the medium-range NOEs $d_{\alpha N(i,i+3)}$ and $d_{\alpha N(i,i+4)}$ indicative of helical secondary structure. The deduced secondary structure is shown in the seventh row. Helices are indicated by boxes, labeled by capital letters. Irregular secondary structure is shown with straight lines. Areas of extended structure that could be identified to participate in β-pleated sheet are indicated with open arrows and labeled with roman numerals (see Figure 8).

and having somewhat downfield $^{13}C_\alpha$ chemical shifts near 63 ppm, in the stromelysin sequence were used to demarcate the regions in which the connected T fragments could be placed. All $^{13}C_\alpha$ chemical shifts were checked against tabulations of ^{13}C chemical shifts by residue type (Olejniczak et al., 1992a) for consistency with the assigned residue type.

At this stage evidence was accumulating that some contiguous stretches of amino acids were missing in the assignment. In these areas, where the cross peaks of some or all experiments were missing or were weaker (R149–F154; H211–A213; T227–D228), the residues are mostly hydrophilic. We concluded that the conditions of experimentation, necessarily chosen for reasons of protein stability and line width optimization (pH 7.0 and 32 °C), were causing transfer of solvent saturation to amide protons by exchange in these apparently exposed areas. In order to obtain the assignments for these areas, we recorded 3D CT-HNCO and CT-HA(CA)CO(N)H experiments and 3D ^{15}N-NOESY-HSQC experiments in which solvent presaturation was avoided by jump–return and gradient techniques, respectively (Figure 1F–H). The latter experiment enabled assignment for the few remaining resonances on the basis of NOE connectivities. The former two experiments enabled assignment of most ^{13}CO resonances. Also, the tuning of delays in HA(CA)CO(N)H was chosen to allow the observation of glycine H_α resonances. The combination of 3D CT-HNCO and HA(CA)CO(N)H was necessary to obtain assignments for those CO resonances for which nearly degenerate ^{15}N–^1H fingerprint resonances exist. The combination of these two experiments is *not* an independent assignment pathway as it relies on the H_α connection. The CO assignments, though listed in Table I, are therefore not included in the assignment diagram. The HN(CA)CO experiment (Clubb et al., 1992b) that *does* give such an independent assignment pathway in combination with the HNCO experiment was of insufficient sensitivity for our sample to be of use.

Figure 6 shows the assignment diagram for SCD. The figure clearly indicates that multiple assignment pathways were found for many of the resonances. All but a few assignments were obtained from long stretches of triple-resonance connections, placed in the sequence using the selective labeling experiments, the glycine identifications, and the proline demarcations. The NOESY connections are mostly confirmatory. Table I lists the obtained assignments.

From the ^{13}C assignments, the deviations of both the carbonyl and carbon α chemical shifts from the chemical shifts of free amino acids, tabulated by Wüthrich (1976) and corrected upward 1.6 ppm for referencing against DSS (V. Thanabal, personal communication), were determined for SCD (Figure 7). This "secondary" shift, with the shift due to residue type subtracted away, has been shown to be statistically correlated with secondary structure (Spera & Bax, 1991).

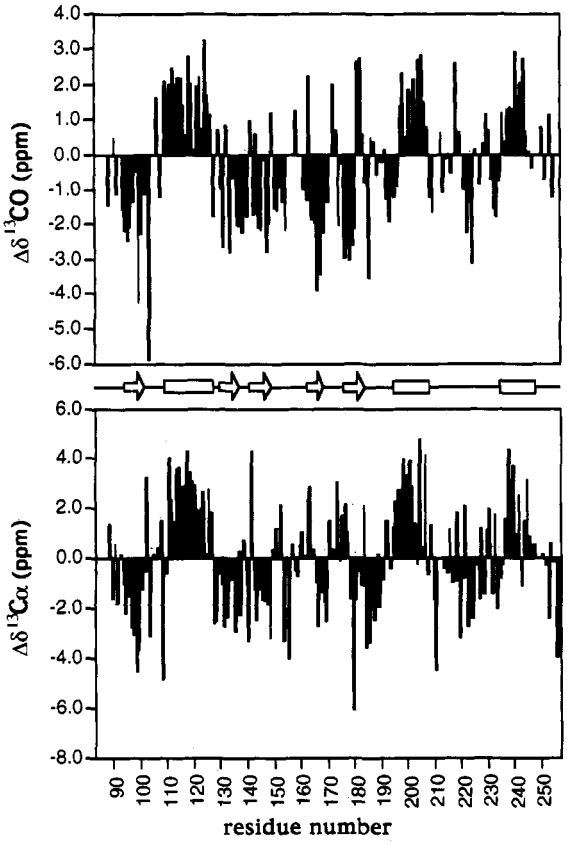

FIGURE 7: Deviations (Δ) from random coil chemical shifts (δ) (Wüthrich, 1976) for the ^{13}CO resonances (top) and $^{13}C_\alpha$ resonances (bottom) of SCD. The secondary structure as derived from NOEs is indicated in the center of the figure with boxes for helices and arrows for the extended structure participating in the five-stranded β-sheet.

Examples of its use previously include Clubb et al. (1993) and Grzesiek et al. (1992b). As seen in Figure 7, positive differences (downfield shifts) of both CO and C_α frequencies well predict the location of the three helices of SCD determined by the characteristic NOE patterns (including lack of sequential $d_{\alpha N}$ NOEs) described below. The negative differences (upfield shifts) of both CO and C_α frequencies are highly correlated with the presence of the sequential $d_{\alpha N}$ NOEs (Figure 6) characteristic of β-strands and other extended structure. For comparison, a sketch of the secondary structure determined by the required NOE patterns (see below) is plotted with the predictive chemical shift deviations in Figure 7.

Secondary Structure. The 3D ^{15}N -resolved NOESY-HSQC spectrum (τ_m = 70 ms) was analyzed for the relative intensity of $d_{\alpha N(i,i+1)}$ and $d_{NN(i,i+1)}$ NOEs. The relative intensities were only obtained for those resonances that were well resolved in 3D space; the assessment was carried out by simple contour-level counting. Extended regions were defined by contiguous regions of strong $d_{\alpha N}$ NOEs. Only those extended regions that could be placed in a β-sheet are indicated. A grid search was conducted in the ^{15}N-resolved NOESY data to identify long-range NOEs between the regions of extended structure to define these strands. Strong $d_{\alpha N(i,j)}$ NOEs, such as those illustrated in Figure 4A, identified anchor points for parallel β-sheet (theoretical distance, for a non-twisted β-sheet, 3.0 Å; Wüthrich, 1986). The NOESY data were then searched for the weaker d_{NN} NOEs (theoretical distance 4.0 Å) also characteristic of this type of secondary structure. Nonsequential $d_{NN(i,j)}$ (theoretical distance 3.3 Å) NOEs together with interstrand $d_{\alpha N}$ NOEs (theoretical distance 3.2 Å) were used as anchor points for the search for antiparallel β-sheet. The very strong $d_{\alpha\alpha}$ NOEs (theoretical distance 2.3 Å) characteristic for antiparallel sheet could not be used as our only sample of ^{13}C-labeled SCD is dissolved in H_2O. Noise from the water resonance makes the identification of these NOEs in our ^{13}C-resolved NOESY spectra (not shown) unreliable. Nevertheless, a sufficient number of $d_{\alpha N}$ and d_{NN} NOEs could be identified to typify the strand of antiparallel sheet in SCD. Thus a single short sheet consisting of four parallel strands and one antiparallel strand could be identified as shown in Figure 8. All regions of well-defined extended structure as delineated in Figure 8 are engaged in sheet except for the short stretches E137–D141 (crossover between β-strands II and III), Q185–D189 (at the end of β-strand V), and L222–L226.

Helices were identified by the presence of strong(er) d_{NN} NOEs, the absence of strong $d_{\alpha N(i,i+1)}$ NOEs, and the presence of stretches of overlapping medium-range $d_{\alpha N(i,i+3)}$ and $d_{\alpha N(i,i+4)}$ NOEs as indicated in Figure 6. The first helix (helix A; residues K110–T128) appears to be a textbook example of amphipathy: 10 hydrophobic residues lie on one side and 9 polar residues at the other side without exception if one assumes 3.6 residues per turn (not shown). This makes it very likely that helix A is an α-helix. This is confirmed by the presence of several $d_{\alpha N(i,i+4)}$ NOEs which are not seen in 3_{10} helices (Wüthrich, 1986). The active-site helix (helix B; residues L195–L209) contains unequal amounts of hydrophobic and polar ones (of which two histidines are believed to coordinate the active site zinc; see below). Its pitch is therefore less easily defined and will have to await the full structure determination. The C-terminal extension of this helix to L209 is indicated by the presence of medium-range NOEs. However, homology with astacin in this area (Bode et al., 1992) would suggest that a turn takes place at Gly 208 in SCD. At the present level of data analysis we cannot exclude that a turn exists for SCD at this location as well; after all, the secondary structure identification methods used are only statistical in nature and are less reliable at the termini of secondary structure elements (Wüthrich, 1986). Definitive statements concerning the extent of this (and other) helices will have to await the full 3D structure determination. The last helix (helix C) has a clear hydrophilic face and a clear hydrophobic face (with the exception of S235 and D238) when built with 3.6 residues per turn, suggesting that helix C is of the α-type as well.

The β-pleated sheet also has clear polarity. In the representation of Figure 8, most residues for which the side chains point down from the page are hydrophobic, whereas the ones pointing up generally are hydrophilic. On this polar face of the β-sheet, the side chains of His 166 and His 179 point up, adjacent to one another. Their proximity suggests that these two histidines, conserved among the matrix metalloproteinases, could coordinate a divalent cation. This cation-binding has been suggested (Gooley et al., 1993) to be the noncatalytic second Zn^{2+}, reported by Salowe et al. (1992). Our data are consistent with this possibility. The hydrophobic face of helix A is expected to pack against the hydrophobic face of the β-sheet, as a crossover from strand I to strand II has to be spanned by this helix. Helix A is sufficiently long to traverse the distance of the crossover between β-strands I and II.

The secondary structure topology of SCD presented herein is in close agreement with that of astacin, a Zn proteinase from the crayfish *Astacus astacus*, for which a high-resolution crystal structure was recently determined (Bode et al., 1992; Gomis-Rüth et al., 1993). The first 70% of SCD contains the

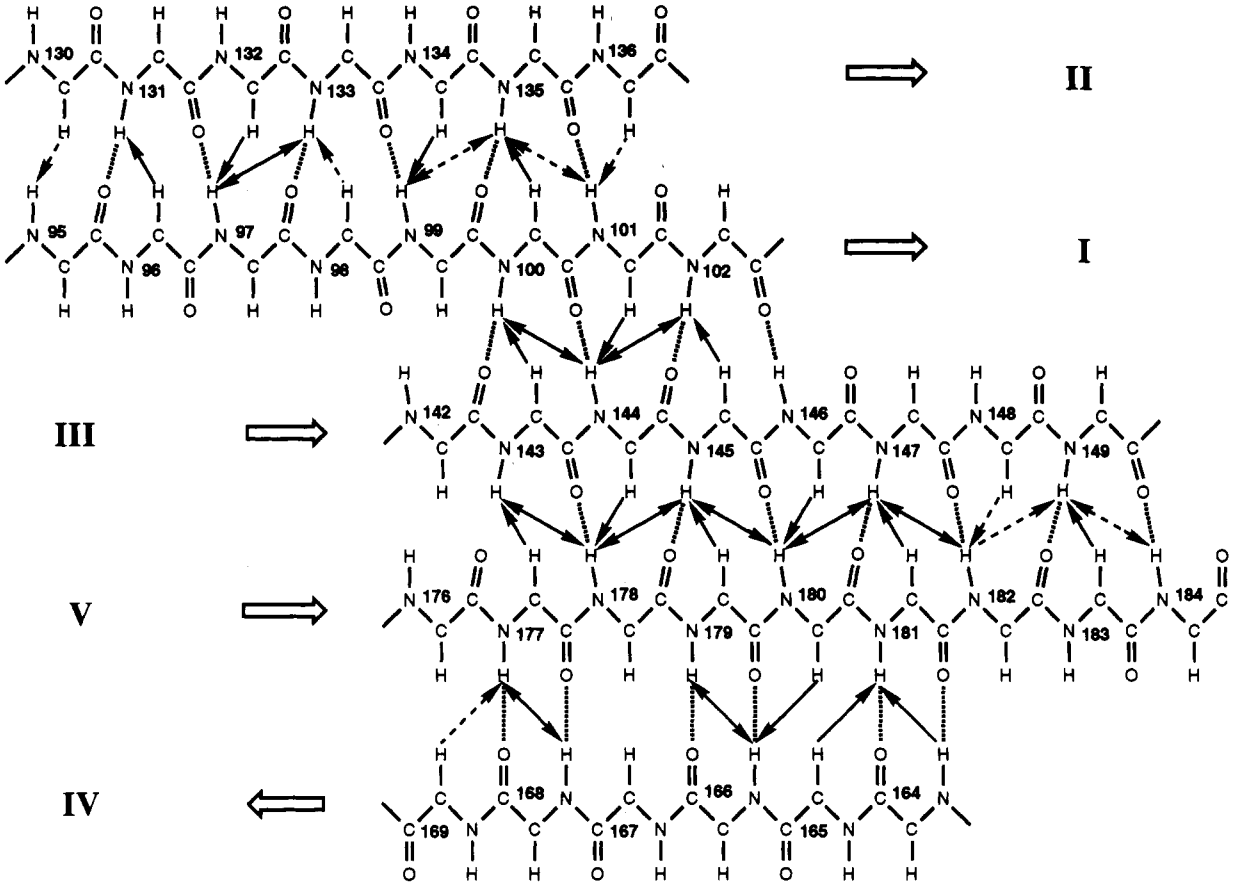

FIGURE 8: Connectivity diagram of the five-stranded mixed β-sheet as delineated from NOEs. Strands I–III and V are parallel while strand IV is antiparallel to strand V. The observed NOEs are indicated by solid arrows. Absence of arrows indicates that no NOE was observed between the involved hydrogen atoms; a dashed arrow indicates that no decision could be made because of overlap in the 3D NMR data. No $d_{\alpha\alpha}$ NOEs were observed at all for reasons described in the text.

highest density of regular secondary structure with the mixed β-sheet of four parallel strands (I–III and V) and one antiparallel strand on the end (IV) as well as two helices. The occurrence and sequential ordering of these elements are identical to those observed in astacin. The last 30% of SCD has mostly irregular features except for the helix C (residues 235–247). This is analogous to astacin except that the irregular domain of astacin is roughly 50 residues longer. The short helix C in this domain of astacin is absent from the catalytic domain of stromelysin-1. Helix D of astacin is equivalent to helix C of SCD (see homology below).

Although the present unavailability of coordinates for astacin makes a precise comparison with SCD impossible, we can make several inferences from the published details. The five-stranded sheet lies on the surface in astacin. The amphipathy for the same sheet in SCD as discussed above suggests that this sheet lies on the surface in SCD as well. The second (Zn-ligating) helix is mostly buried in astacin; the location of this helix in SCD appears to be the same following from its hydrophobic character. The first and last helices lie on the surface in astacin. The observed amphipathy of these same helices in SCD makes a similar location probable. The striking similarity in secondary structure of SCD with astacin as discovered here reveals some sequence identities and homologies previously gone unrecognized. Previously, the sequence similarities between the matrix metalloproteinases and astacin had been described only for the active-site helix which contains ligands to the catalytic zinc (helix B; Bode et al., 1992). In fact, the first and last helices of astacin and SCD also show particularly striking commonalities in sequence and amphipathy. Listed are the homologous first and last helices of stromelysin catalytic domain and of astacin with identical residues in bold:

```
SCD helix A:      110 K D A V D S A V E K A L K V W E E V T 128
Astacin helix A:   23 S G A D Q S A I L S G M Q E L E E K T  41
```

Hirose et al. (1993) have recently shown using site-directed mutagenesis that the aspartate in neutrophil collagenase (Asp 253 in their numbering) corresponding to Asp 238 of SCD in helix C is crucial for proteolytic activity. The residue is conserved not only among the mammalian matrix metalloproteinases but also with astacin as is revealed by the above alignment of helices. Hirose et al. (1993) proposed that this aspartate serves as a ligand to a divalent cation, but we note that Gomis-Rüth et al. (1993) did not report the presence of such a cation in the astacin structure, putting some doubt on the hypothesis of Hirose et al. (1993).

At present, we cannot confidently make a similar residue-to-residue alignment between the residues in the five-stranded sheets of astacin and SCD. We do not detect homology as clear as for the helices on the primary level in the region of the sheet to complement the secondary homology and topology there. Initial alignment efforts show that a five-residue insertion is present in SCD between β-strand I and helix A as compared to astacin. About 12 residues are inserted between strands III and IV, and about five residues are inserted between β-strand V and helix B. On the basis of sequence alignments of matrix metalloproteinases of Docherty and Murphy (1990), the site of the insertion of the fibronectin-like domain in the gelatinases is expected to lie between strand V and helix B.

Even at the level of comparison without coordinates, these observations of primary, secondary, and topological homologies make it very likely that the tertiary structures of astacin and SCD are also related. This is remarkable considering that the level of overall amino acid homology between these molecules is clear only for the helices. Of particular interest is of course to identify the coordination of the active-site zinc. The present study agrees with the hypothesis, based on localized homology with the known structure of astacin (Bode et al., 1992), that residues His 201 and His 205 of the active-site helix as well as His 211 just beyond this helix coordinate the zinc. The identification of the fourth Zn-coordinating ligand, which in astacin comes from the irregular domain of the molecule, may have to await the determination of the full tertiary structure of SCD. We are in the progress of obtaining the side-chain NMR assignments for the molecule in order to do so.

CONCLUSIONS

We have reported virtually complete assignments for the main-chain ^{13}C, ^{15}N, and ^{1}H resonances for the catalytic domain of stromelysin. The assignments were predominantly obtained from triple-resonance 3D experiments. The secondary structure of the molecule was determined from analysis of the 3D ^{15}N-resolved NOESY spectrum. The secondary structure topology of SCD was found to consist of a five-strand mixed β-sheet consisting of four parallel strands (95–102, 130–136, 143–149, and 177–184), one antiparallel strand (164–168), and three helices (110–128, 195-209, 235–247). This topology is nearly identical to that found for astacin, a Zn proteinase for which the tertiary structure is known from X-ray diffraction data.

ACKNOWLEDGMENT

We are most grateful for the efforts of Dr. Ananya Majumdar in writing extensions to the NMR processing programs, particularly an interface for rapid switching between many spectra to expedite assignments. We appreciate advice from Mr. Mark Fischer. We thank Dr. Mark Friedrichs for the gift of a routine for complex linear prediction. S.R.V.D. receives support from Grant PF-4056 from the American Cancer Society.

REFERENCES

Basset, P., Belloca, J. P., Wolf, C., Stoll, I., Hutin, P., Limacher, J. M., Podhajces, O.Y., Chenard, M. P., Rio, M. C., & Chambon, P. (1990) *Nature 348*, 69–70.

Bode, W., Gomis-Rüth, F. X., Huber, R., Zwilling, R., & Stöcker, W. (1992) *Nature 358*, 164–167.

Boucher, W., Laue, E. D., Campbell-Burk, S., & Domaille, P. J. (1992) *J. Am. Chem. Soc. 114*, 2262-2264.

Clark, I. M., & Cawston, T. E. (1989) *Biochem. J. 263*, 201–206.

Clavel, C., Polette, M., Doco, M., Benninger, I., & Berembaut, P. (1992) *Bull. Cancer 79*, 261–270.

Clore, G. M., & Gronenborn, A. M. (1991) *Prog. NMR Spectrosc. 23*, 43–92.

Clore, G. M., Wingfield, P. T., & Gronenborn, A. M. (1991) *Biochemistry 30*, 2315–2323.

Clubb, R. T., Thanabal, V., Osborne, C., & Wagner, G. (1991) *Biochemistry 30*, 7718–7730.

Clubb, R. T., Thanabal, V., & Wagner, G. (1992a) *J. Biomol. NMR 2*, 203–210.

Clubb, R. T., Thanabal, V., & Wagner, G. (1992b) *J. Magn. Reson. 97*, 213–217.

Clubb, R. T., Thanabal, V., Fejzo, J., Ferguson, S. B., Zydowsky, L., Baker, C. H., Walsh, C. T., & Wagner, G. (1993) *Biochemistry 32*, 6391–6401.

DiPasquale, G., Caccese, R., Pasternak, J., Conaty, J., Hubbs, S., & Perry, K. (1986) *Proc. Soc. Exp. Biol. Med. 183*, 262–267.

Docherty, A. J. P., & Murphy, G. (1990) *Ann. Rheum. Dis. 49*, 469–479.

Emonard, H., & Grimaud, J. A. (1990) *Cell. Mol. Biol. 36*, 131–153.

Engel, G., Popowicz, P., Norling, H., Svensson, C., Auer, G., Akusjarvi, G., & Linder, S. (1992) *Int. J. Cancer 51*, 761–766.

Enghild, J. J., Salvesen, G., Brew, K., & Nagase, H. (1989) *J. Biol. Chem. 264*, 8779–8785.

Fesik, S. W., & Zuiderweg, E. R. P. (1988) *J. Magn. Reson. 78*, 588–593.

Fesik, S. W., & Zuiderweg, E. R. P. (1990) *Q. Rev. Biophys. 23*, 97–131.

Flannery, C. R., Lark, M. W., & Sandy, J. D. (1992) *J. Biol. Chem. 267*, 1008–1014.

Gomis-Rüth, F. X., Stöcker, W., Huber, R., Zwilling, R., & Bode, W. (1993) *J. Mol. Biol. 229*, 945–968.

Gooley, P. R., Johnson, B. A., Marcy, A. I., Salowe, S. P., & Cuca, G. C. (1993) *J. Cell. Biochem., Suppl. 17C*, 274.

Grzesiek, S., & Bax, A. (1992) *J. Magn. Reson. 96*, 432–440.

Grzesiek, S., & Bax, A. (1993) *J. Biomol. NMR 3*, 185–204.

Grzesiek, S., Dobeli, H., Gentz, R., Garotta, G., Labhardt, A. M., & Bax, A. (1992) *Biochemistry 31*, 8180–8190.

Heath, T. G., Thanabal, V., & Ye, Q.-Z. (1993) *Biotechnol. Tech. 7*, 367–372.

Hibler, D. W., Harpold, L., Dell'Acqua, M., Pourmotabbed, T., Gerlt, J. A., Wilde, J. A., & Bolton, P. H. (1989) *Methods Enzymol. 177*, 74–86.

Hirose, T., Patterson, C., Pourmotabbed, T., Mainardi, C. L., & Hasty, K. A. (1993) *Proc. Natl. Acad. Sci. U.S.A. 90*, 2569–2573.

Holmes, P., & Matthews, B. W. (1982) *J. Mol. Biol. 160*, 623–639.

Ikura, M., Kay, L. E., & Bax, A. (1990) *Biochemistry 29*, 4659–4667.

Ikura, M., Clore, G. M., Gronenborn, A., Zhu, G., Klee, C. B., & Bax, A. (1992) *Science 256*, 632–638.

Kay, L. E., Ikura, M., Tschudin, R., & Bax, A. (1990) *J. Magn. Reson. 89*, 496–514.

Kusukawa, J., Sasaguri, Y., Shima, I., Kameyama, T., & Morimtsu, M. (1992) *J. Oral Pathol. Med. 21*, 221–224.

Levitt, M. H., & Freeman, R. (1981) *J. Magn. Reson. 43*, 502–507.

Levy, G. C., & Lichter, R. L. (1979) *Nitrogen-15 Nuclear Magnetic Resonance Spectroscopy*, John Wiley & Sons, New York.

Lowry, C. L., McGeehan, G., & LeVine, H., III (1992) *Proteins: Struct., Funct., Genet. 12*, 42–48.

Majumdar, A., & Zuiderweg, E. R. P. (1993) *J. Magn. Reson. B 102*, 242–244.

Marcy, A. I., Eiberger, L. L., Harrison, R., Chan, H. K., Hutchinson, N. I., Hagmann, W. K., Cameron, P. M., Boulton, D. A., & Hermes, J. D. (1991) *Biochemistry 30*, 6476–6483.

Marion, D., Driscoll, P. C., Kay, L. E., Wingfield, P. T., Bax, A., Gronenborn, A. M., & Clore, G. M. (1989a) *Biochemistry 28*, 6150–6156.

Marion, D., Ikura, M., Tschudin, R., & Bax, A. (1989b) *J. Magn. Reson. 85*, 393–399.

Matrisian, L. M. (1992) *BioEssays 14*, 455–463.

Meadows, R. P., Nettesheim, D. G., Xu , R. X., Olejniczak, E. T., Petros, A. M., Holzmann, T. F., Severin, J., Grubbins, E., Smith, H., & Fesik, S. W. (1993) *Biochemistry 32*, 754–765.

Messerle, B. A., Wider, G., Otting, G., Weber, C., & Wüthrich, K. (1989) *J. Magn. Reson. 85*, 608–613.

Miyazaki, K., Umenishi, F., Funahashi, K., Koshikawa, N., Yasumitsu, H., & Umeda, M. (1992) *Biochem. Biophys. Res. Commun. 185*, 852–859.

Muchmore, D. C., McIntosh, L. P., Russell, C. B., Anderson, D. E., & Dahlquist, F. W. (1989) *Methods Enzymol. 177*, 44–73.
Murphy, G. M., & Docherty, A. J. P. (1992) *Am. J. Resp. Cell Mol. Biol. 7*, 120–125.
Nagase, H., Enghild, J. J., Suzuki, K., & Salvesen, G. (1990) *Biochemistry 29*, 5783–5789.
Nagase, H., Ogata, Y., Suzuki, K., Enghild, J. J., & Salveson, G. (1991) *Biochem. Soc. Trans. 19*, 715- 718.
Okada, Y., Shinmei, M., Tanaka, O., Naka, K., Kimura, A., Nakanishi, I., Bayliss, M. T., Iwata, K., & Nagase, H. (1992) *Lab. Invest. 66*, 680–690.
Olejniczak, E. T., Xu, R. X., & Fesik, S. W. (1992a) *J. Biomol. NMR 2*, 655–659.
Olejniczak, E. T., Xu, R. X., Petros, A. M., & Fesik, S. W. (1992b) *J. Magn. Reson. 100*, 444–450.
Peng, J. W., & Wagner, G. (1992) *J. Magn. Reson. 98*, 308–332.
Polette, M., Clavel. C., Muller, D., Abecassis, J., Binninger, I., & Birembaut, P. (1991) *Invasion Metastasis 11*, 76–83.
Salowe, S. P., Marcy, A. I., Cuca, G. C., Smith, C. K., Kopka, I. E., Hagmann, W. K., & Hermes, J. D. (1992) *Biochemistry 31*, 4535–4540.
Shaka, A. J., Keeler, J, Frenkiel, T., & R. Freeman. (1983) *J. Magn. Reson. 52*, 335–338.
Spera, S., & Bax, A. (1991) *J. Am. Chem. Soc. 113*, 5490–5492.
Sreenath, T., Matrisian, L. H., Stetler-Stevenson, W., Gattoni-Celli, S., & Pozatti, R. O. (1992) *Cancer Res. 52*, 4942–4947.
Stetler-Stevenson, W. G. (1990) *Cancer Metastasis Rev. 9*, 289–303.
Stöcker, W., Ng, M., & Auld, D. S. (1990) *Biochemistry 29*, 10418–10425.
Stockman, B., Nirmala, N. R., Wagner, G., Delcamp, T. J., DeYarman, M. T., & Freisheim, J. H. (1992) *Biochemistry 31*, 218–229.
Tabor, S., & Richardson, C. C. (1985) *Proc. Natl. Acad. Sci. U.S.A. 82*, 1074–1078.
Theriault, Y., Logan, T. M., Meadows, R.,Yu, L., Olejniczak, E. T., Holzman, T. F.,Simmer, R. L., & Fesik, S. W. (1993) *Nature 361*, 88–91.
Van Doren, S. R., & Zuiderweg, E. R. P. (1993) *J. Magn. Reson. A 104*, 222–225.
Walakovits, L. A., Moore, V. L., Bhardwaj, N., Gallick, G. S., & Lark, M. W. (1992) *Arthritis Rheum. 35*, 35–42.
Woessner, J. F., Jr. (1991) *FASEB J. 5*, 2145–2154.
Wüthrich, K. (1976) *NMR in Biological Research: Peptides and Proteins*, North Holland/American Elsevier, New York.
Wüthrich, K. (1986) *NMR of Proteins and Nucleic Acids*, John Wiley, New York.
Ye, Q.-Z., Johnson, L. L., Hupe, D. J., & Baragi, V. (1992) *Biochemistry 31*, 11231–11235.
Ye, Q.-Z., Johnson, L. L., Noadan, I., Hupe, D. J., & Hupe, L. (1993) *J. Med. Chem.* (submitted for publication).
Zhu, G., & Bax, A. (1990) *J. Magn. Reson. 90*, 405–410.